Back to Ground Zero: A study on rear passivated thin-CIGS solar cells

Sunil Suresh

TU Delft · imec

Back to Ground Zero: A study on rear passivated thin-CIGS solar cells

by

Sunil Suresh

in partial fulfillment of the requirements for the Master of Science

Sustainable Energy Technology

at the Delft University of Technology,
to be defended publicly on Monday July 16, 2018 at 1:00 PM.

Student number:	4620216	
Project duration:	November 1, 2017 – June 30, 2018	
Supervisors:	Prof. dr. Bart Vermang	imec, Hasselt University
	Dr. Olindo Isabella	TU-Delft
Thesis committee:	Prof.dr. Miro Zeeman	TU-Delft
	Prof. dr. Bart Vermang	imec, Hasselt University
	Dr. Olindo Isabella	TU-Delft

This thesis is confidential and cannot be made public until December 31, 2018.

An electronic version of this thesis is available at `http://repository.tudelft.nl/`.

TU Delft Delft University of Technology

Abstract

Having an absorber layer thickness below 1 μm for a regular copper indium gallium di-selenide (CIGS) solar cell reduces the pathways for electron collection which lead to reduced recombination in the bulk absorber layer. Additionally, it reduces material costs and production time. Yet, having such a thin absorber reduces the cell efficiency significantly, mainly due to incomplete light absorption and high Mo/CIGS rear-surface recombination [61]. The aim of this research is to implement some innovative rear surface modifications for a <500 nm thick CIGS absorber layer to reduce these affects: a passivation layer to reduce the back-surface recombination and point contact openings using nano-particles (NPs) (CdS, Ag, etc.) to create electrical contacts, with some NPs also improving the optical confinement. For example, one approach is to use a layer of thermally evaporated and uniformly deposited Ag, which is then annealed to create Ag NPs with typical diameters of 300 to 450 nm. An Al_2O_3 layer is used to passivate the Mo/CIGS rear surface which also prevents the NPs from completely dissolving into the absorber during the absorber deposition. The implementation of all these rear-surface modifications and their impact on the electrical performance of the CIGS solar cell will be discussed and analyzed in this paper. This work received funding from the European Union's H2020 research and innovation program under grant agreement No. 715027.

Contents

List of Figures

List of Tables

Nomenclature

A	Ideality Factor
AZO	Aluminium doped Zinc Oxide
c-Si	Crystalline silicon solar cells
CBD	Chemical Bath Deposition
CIGS	$Cu(Ga,In)Se_2$
AIGS	Ag $(In_{1\_y}Ga_y)Se_2$
Solar device	Group of several solar cells
Efficiency	Power conversion efficiency
Eg	Bandgap energy
EQE	External quantum efficiency
FF	Fill factor
i-ZnO	Intrinsic Zinc Oxide
J-V	Current (density)-voltage
IVT	Temperature-dependent current (density)-voltage
J_0	Dark saturation current (density)
J_{SC}	Short-circuit current
V_{OC}	Open-circuit voltage
CV	Capacitance-voltage
PL	Photo-luminescence
PV	Photovoltaics
R_{ser}	Series resistance
R_{shunt}	Shunt resistance
N_{it}	Interface trap density
SLG	Soda Lime Glass
STC	Standard Test Conditions
TCO	Transparent Conductive Oxide
TRPL	Time-resolved photoluminescence
abs.	Absolute
A_X	'A' element vacancy defect
A_B	Anti-site lattice defect of 'A' atom in 'B'

Preface

Firstly, I would start by expressing my sincere gratitude to Prof. dr. Bart Vermang for your insightful comments, patience, time and belief in me. I am also grateful to Dr. Jessica De Wild for being critical, appreciative and more importantly my daily supervisor and Dr. Marc Meuris, for providing me with the support, guidance and invaluable learning experience at imec. I would like to thank the group members of the ATFPV team namely, Dr. Guy Brammertz and Thierry Kohl for helping me with their prompt suggestions and MATLAB coding. I am also thankful to Arsalan Razzaq, Imre Horvath and Jinyon Cho, for their timely guidance and Kim Baumans, for training me in most of the equipment I used.

I am also grateful to Prof. dr. Miro Zeeman and Dr. Olindo Isabella, members of my thesis committee, for their support. Finally, I must express my gratitude to my family in India, especially amma (for making me who I am today and being patient with me when I struggled to write basic alphabets), appa (for believing in me and guiding me) and Sanju (for being a very supportive and enthusiastic elder brother and someone to look up to). I would like to dedicate my thesis to both my late grandmothers; thank you patti(s) for all your prayers and enlightening conversations. A big shout out to my friends Abi (cheers to our endless debates on solar energy and life in general), Manoj (for your calm and understanding nature), Ghanshyam (for all the "mindful" conversations and providing me a house to stay and food to eat during my short trips to Delft) and many more for making life in Delft memorable and enjoyable.

Sunil Suresh
Delft, July 2018

Cover page: Onyx thin-film solar modules with varying degrees of transparency at the Food Market of Bejar, Salamanca.

1 Introduction

1.1. Renewable Energy-The need

> "The spread of civilization may be likened to a fire; first, a feeble spark, next a flickering flame, then a mighty blaze, ever increasing in speed and power"
> *-Nikola Tesla*

Before the oil embargo of 1973, before the word “green” became a badge of good stewardship, University of Delaware's Institute of Energy Conversion (IEC) built “Solar One” (Figure 1.1), an experimental house that used solar energy for both its heating and electrical requirements [1]. It used a CdS/Cu_2S solar cell, the first major thin film solar cell and demonstrated the practical potential of solar energy. Its glory days are past, but it still stands as a humble testament to the potential of this inexhaustible and free source of energy for the planet.

Figure 1.1: An image of Solar One, a house that used solar energy for its heating and electrical requirements. It was built with support from Delmarva Power and Light by the Institute of Energy Conversion in 1973 [1].

Mankind's thirst for power has touched record levels - we have consumed more than 135 billion tonnes of crude oil to heat our homes, drive our vehicles and fuel our power plants in the last 100 years [15]. In the year 2017, 62% of the primary energy consumed came from oil and coal consumption (Figure 1.2), with renewables contributing a meagre 3% worldwide (excluding hydro power) [10].

Nuclear energy could be an alternative less pollutive energy source however, radioactive contamination and waste disposal is expensive and potentially life threatening; the Fukushima nuclear accident in Okuma for instance showed the devastating effects of a reactor breakdown with the human and economic cost being immense. Access to cheap and clean energy is essential for the development of modern economies, yet, ever increasing energy demands, depleting oil reserves, pollution and energy security have led to significant vulnerabilities in the current energy mix. This threat to the current energy system gives a rationale for investing in renewable energy. Renewable energy, generated from renewable sources (sunlight and geothermal energy, others like wind and hydro-energy are indirect forms of solar energy), is replenished on a human timescale. The mitigation of climate change has been the main justification behind renewable energy however, it is certainly not the only motive. For instance, reducing the CO_2 emissions due to the increased use of renewables decreases local air pollution. This reduces the health issues surrounding it, forcing the Chinese government for example, to invest about 360 billion dollars towards renewable energy in early 2017 [36]. Secondly, it improves the energy security in a country by improving it's resilience in face of predicted climate change impacts.Lastly, with the economies around the world facing a reduced growth, development of renewable energies creates local value and jobs, offering a way to increase the income of people and contribute to industrial development in a sustainable and clean fashion. According to the latest World Energy report by British Petroleum, it is now the fastest growing source of energy, growing at the rate of 7.1% every year, reaching up to 10% of the primary energy source by 2035 [10].

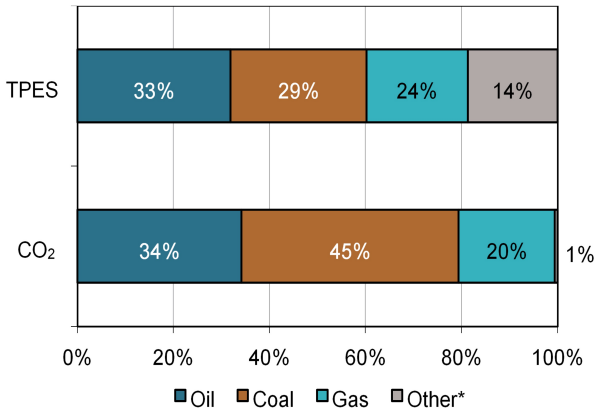

Figure 1.2: In the year 2017, a meagre 14% of the world's total primary energy supply (TPES) came from renewable energy sources. Fossil fuels still dominate the total fuel share (worldwide) and contributed to nearly 99% of the total CO_2 emissions [10].

Among the many renewable sources of energy, solar energy has the greatest biophysical potential and power density [58]. Earth is bathed in unlimited energy from the sun delivering power that humankind consumes over the course of a whole year every hour [58]. To utilize the energy of the sun, photovoltaic (PV) cells are used. They convert solar energy to direct current electricity. These cells are reliable, noiseless, need no fuel, and produce electricity without releasing any greenhouse gases. The most significant boost to the commercial PV industry is its plummeting cost, with the price of solar panels falling by nearly 80% in the last ten years [58].

1.2. Photovoltaics Today

Currently, the field of photovoltaics comprises of wafer based silicon solar cells with an absorber thickness of roughly 200 μm and thin film solar cells (TF) like perovskites and kesterites with absorber thicknesses of about 3 μm for complete light absorption.

Silicon (c-Si) technology dominates over 90% of the commercial PV market [48] due to its cheap, efficient and environmentally well-suited device properties (Figure 1.3).

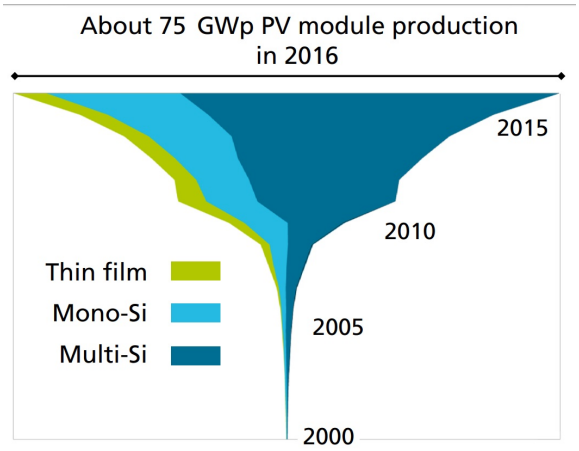

Figure 1.3: The annual energy production from PV modules for the year 2016. Thin-film technologies contributed to roughly 6% of the total energy production [23].

Still, when compared with c-Si technology, there are still several areas where alternative thin-film solar cells provide better material related properties such as:

- **Absorption:** Silicon (Si), an indirect band gap semiconductor has a relatively poor absorption coefficient (around 10^3 cm^{-1} for wavelengths >600 nm). Consequently, it absorbs solar spectrum in the near infrared region poorly, effectively needing about 60-100 μm for sound incident light absorption (terrestrial applications). Furthermore, current wafer sawing methods limit the minimum thickness to around 180 μm making it bulky and less flexible. Besides, kerf losses lead to significant silicon wastage (can be recycled). Accordingly, c-Si is primarily used in solar farms and roof-tops. Instead, most of the thin-film absorber materials have a much higher absorption coefficient (10^5 cm^{-1} in the 1.0-1.3 eV region) needing only 2-3 μm for complete light absorption. This makes them significantly lighter and more flexible (when grown on polymer substrates for example), properties which are suited for building integrated photovoltaic system (BIPV) based applications. This includes usage in building facades and windows that need a certain level of transparency, aesthetic beauty and light weight.

- **Material:** Si is the one of the amplest element available on the earth's crust, second only to oxygen. However, it is present in the form of SiO_2 or silica, which is a very stable material. Obtaining electronic grade Si from silica can be an expensive and energy intensive process [65]. Alternatively, TF can be fabricated on lower thermal budgets and by simpler production techniques. For example, newer materials like perovskites, organic and quantum dot solar cells can be produced by solution based processing techniques [58]. Furthermore, c-Si modules function optimally under direct solar radiation thus, for maximum power production, sun tracking systems are essential. This increases the energy payback period for conventional silicon modules. For comparison, a mono-Si module has a payback period of 2.12 years when compared to 0.78 years for a CIGS module under 1700 $kWhm^{-2}$ solar irradiation per year [6].

- **Bandgap engineering:** For single junction devices, an absorber band gap of either 1.10 eV or 1.35 eV yields the maximum theoretical efficiency or the Shockley-Queisser limit of 33.5% [57]. Multi-junction solar cells on the other hand can theoretically achieve efficiencies of close to 86% under suitable light conditions [14].

Essential to obtain multi-junction solar cells is the ability to tune the bandgap i.e. change the bandgap of the material by controlling the chemical composition of its constituent materials. c-Si technology does not have much flexibility in this aspect (other than amorphous silicon) while thin-film materials like chalcopyrites and kesterites have tunable bandgaps based on the concentration of its constituent elements. In the chalcopyrite copper indium gallium diselenide (CIGS) for example, altering the amount of gallium or replacing the copper (Cu) with silver (Ag) among others, could lead to an increased band-gap, paving way for tandem cell applications.

1.2.1. CIGS solar cells

At the time of writing this paper, CIGS solar cells reached a record conversion efficiency of 22.9%, the highest among any of the currently used poly-crystalline thin film materials [46]. A high light absorption coefficient and direct band gap means only 1-3 μm of active layer is sufficient for complete light absorption [24]. Correspondingly, CIGS modules are flexible, light-weight and can be designed in an aesthetically pleasing manner, making it suitable for applications in the BIPV market. Owing to its low-temperature coefficient, CIGS cells are more resistant to adverse climatic variations such as hot temperatures and diffused light conditions that would otherwise affect cell performance [44]. With the possibilities for roll to roll manufacturing, CIGS solar devices have showed high volume growth reaching up to 1.1 GWp recently [23].

Considering the vast potential of CIGS technology, currently, research is being carried out to increase its global competitiveness in the solar energy market for Gigawatt levels of energy production. Apart from high module efficiencies, reduced cost and increased throughput are equally important for the scalability and commerciality of this technology. Presently, the CIGS manufacturing industry faces the issue of scalability; CIGS technology contributes to less than 2% of the total PV market share (for the year 2017) [23].This stems from the use of the metals indium and gallium, which are both expensive and scarce (indium has an estimated abundance of 0.049 ppm making it rarer than silver (Ag) [12]). The European Commission Report [3] estimates both the metals to be critical raw materials owing to their supply risk and demand. Consequently, fluctuating gallium costs (Table 1.1) and rapidly increasing indium demand (widespread applications in touchscreen and flat panel industry) have raised serious questions on the economics of the constituent elements. Besides, for commercial CIGS modules, the average efficiencies are about 15-17% (lab scale devices have ~ 22%).

Table 1.1: Price fluctuation for the metals In and Ga [37].

Resource	Price ($/kg) 2014	2015	Price Fluctuation 2010-2105 ($/kg)	Major uses
In	705	540	200-800	ITO
Ga	365	285	150-1000	GaN

Major cost reductions and increased throughput can be achieved by reducing the absorber thickness. To put this in context, the cost for In and Ga as calculated by Horowitz et al. [20] was 2.6 €/m^2 (18.3 €/kW) for a 2000 nm thick standard CIGS absorber, but the same for a 400 nm absorber layer was 0.6 €/m^2 (4.6 €/kW). Yet, if the thickness of the absorber is lesser than 1 micrometer, the electrical performance of the CIGS device degrades (Figure 1.4) due to incomplete absorption of incoming photons, back contact recombination and shunting issues [33]. This outweighs the benefits of having a thinner layer; for a 1% drop in the efficiency, the cell cost would shoot up by 35 €/kW [20]. Subsequently, the CIGS industry's focus has gradually shifted towards research on thin-CIGS solar cells i.e. to make thin absorber layer CIGS (>400 nm and <1000 nm) with high efficiencies.

Although at first reading, it may seem unusual or surprising that a reduction in the absorber thickness is needed, many research institutions like NREL [9], Angstrom Solar Center [61] and ZSW [53] have recognized the need to reduce the absorber layer thickness and are now focusing their research towards improving the electrical characteristics of a thin CIGS solar cell. This move is due to several advantages such as reduced bulk recombination losses, its dependence to the metal market and reduced manufacturing costs. The latter two will be critical parameters to make CIGS more competitive in the PV market [49].

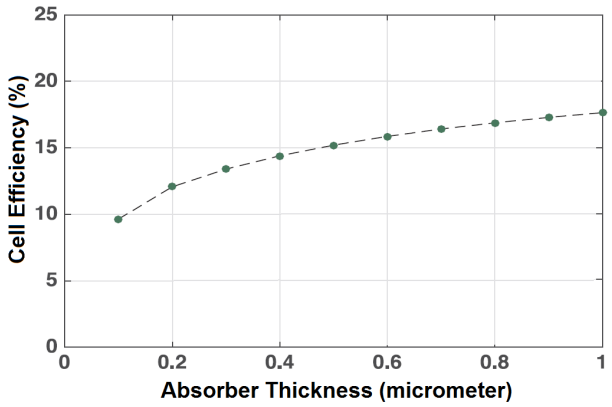

Figure 1.4: Simulated effects of a reduced absorber thickness on cell efficiency. The loss is efficiency is attributed to inadequate light absorption and increased interface recombination [61].

1.3. Motivation

Elements essential for fabrication of sound photovoltaic devices are: suitable cell architecture for efficient carrier collection and stable band structure. Given the complex nature of the ternary CIGS, the motive of this research work was to contribute to development of advanced cell architectures for passivated thin-CIGS devices, with special focus on the rear surface of the cell. This includes the implementation of an aluminum oxide layer (for rear surface passivation) and generation of point nano-contacts (for electrical contacts) in a reliable and reproducible manner. The motive behind the development of such advanced architectures is to bring down cell costs (by reducing the absorber thickness) and at the same time keep sound cell efficiencies. Furthermore, an attempt was made to introduce metals like silver into the absorber of a rear passivated device to fabricate higher band-gap thin-film materials. Accordingly, initial experiments were performed to understand the cell structure and create baseline parameters for reproducible device fabrication. Subsequently, novel improvements were attempted to study its impact on the cell architecture.

1.3.1. Passivated CIGS cell architecture

The cell architecture was altered (when compared to a standard CIGS solar cell) to incorporate a passivation layer. Figure 1.5 illustrates the final cell architectures for the two-modified devices fabricated in this thesis along with a standard reference device. All the devices use a standard molybdenum back contact (high thermal stability and work function of 4.6 eV). An ultra-thin aluminium oxide layer is used to passivate the rear interfaces for the rear-modified devices. A single-stage evaporation process (no-Ga grading) was used to deposit the p-type CIGS semiconductor. Since the bulk CIGS is of p-type conductivity, an n-CdS buffer was deposited to create a p-n junction (CdS also passivates the front surface). A transparent conducting oxide layer was used consisting of intrinsic ZnO and Al-doped ZnO. Further, a nickel doped aluminium grid was deposited to aid in the charge carrier collection.

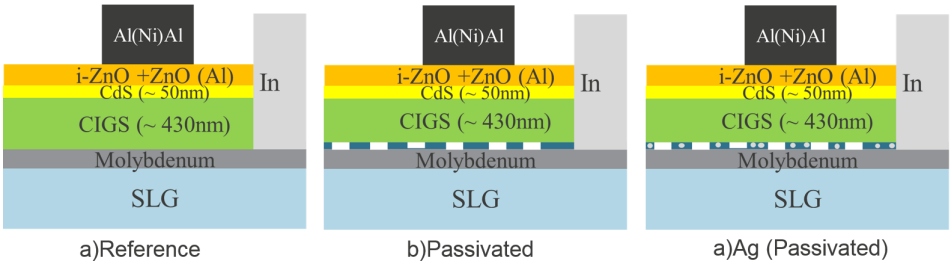

Figure 1.5: An illustration of the cell architecture used in the present work.

Lastly, indium was soldered on to the top surface of the solar device (scrapping off all the layers except Mo) to set up an electrical link between the measuring probes and back contact. Chapter 2 provides a more detailed insight on the fabrication process. A sample device is shown in Figure 1.6.

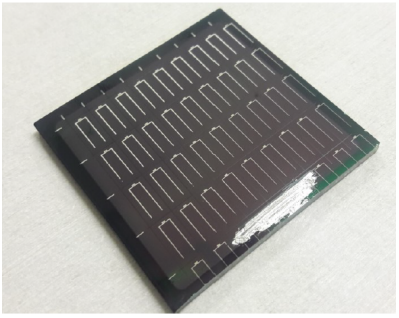

Figure 1.6: A sample 5 cm × 5 cm CIGS device with 32 cells.

1.3.2. Thesis Outline

This report is divided into 6 chapters explained as follows: **Chapter 2** gives a detailed overview of the CIGS crystal structure and state of art research. Important aspects of the cell like lattice structure, defect states, doping etc. have been explained to a certain extent. Doing so further explains the motivation for certain experiments conducted in this work. **Chapter 3** explains the various steps involved in cell fabrication and also the characterization techniques utilized. Since the cell architecture is modified when compared to the standard CIGS device, certain aspects such of the cell such as deposition of the passivation layer has been explained in more detail. The focus of **Chapter 4** is on reducing the rear interface recombination of a thin-film CIGS solar cell. Attempts were made via innovative rear surface modifications to a 430 nm thick CIGS absorber layer: a passivation layer (Al_2O_3) to reduce the back-surface recombination and point contact openings using nanoparticles (NPs) to create electrical contacts. Extensive studies have not been carried out yet with nano-particle based point contact opening for a rear passivated thin-CIGS device. This makes this work beneficial to the research community. The highest V_{OC} obtained for the passivated device was 604 mV which is on par with the record V_{OC} for such thin-CIGS devices. The work carried out in chapter 4 and 5 was presented as a poster at the E-MRS (spring 2018) meet and is now under review for publication as a manuscript in Physica Solidi Status journal. **Chapter 5** focuses on attempts carried out to introduce silver into the absorber in a controlled manner. The addition of silver is particularly interesting as it increases the bang-gap of the material and reduces the disorder on the crystal structure. Again, this would be useful for the scientific community as Ag based CIGS devices haven't been studied extensively. **Chapter 6** summarizes the experimental findings and provides some recommendations.

2

CIGS solar cells

2.1. Crystal structure and defects

CIGS is an alloy of the ternary chalcopyrites $CuInSe_2$ and $CuGaSe_2$, with a gallium by gallium plus indium ratio (GGI) being close to 0.3 [56]. The term "chalcopyrite" comes from the mineral chalcopyrite $CuFeS_2$, which is commonly found copper-iron ore. Alloying of Ga into the $CuInSe_2$ complex (i.e. replacing In with Ga) increases the band gap of the material from 1.04 to 1.67 eV due to the joint effects of spin orbit coupling and tetragonal crystal field [28]. Its structure is similar to that of a zincblende (Figure 2.1a), which consists of two interpenetrating face centered cubic lattices, one occupied by cations and the other by anions [56]. Likewise, in a tetrahedral chalcopyrite like CIGS, the cations are substituted by two cations of higher valency (In or Ga) and one cation with lower valency (Cu) in an ordered manner (Figure 2.1b). Thus, its structure is a ternary analogue of a zincblende structure consisting of a primitive cell with eight atoms and reduced symmetry owing to the three-different kinds of cations in the structure. The observed oxidation states for the cations are +1(Cu) and +3 (In and Ga) and -2 for the Se anion.

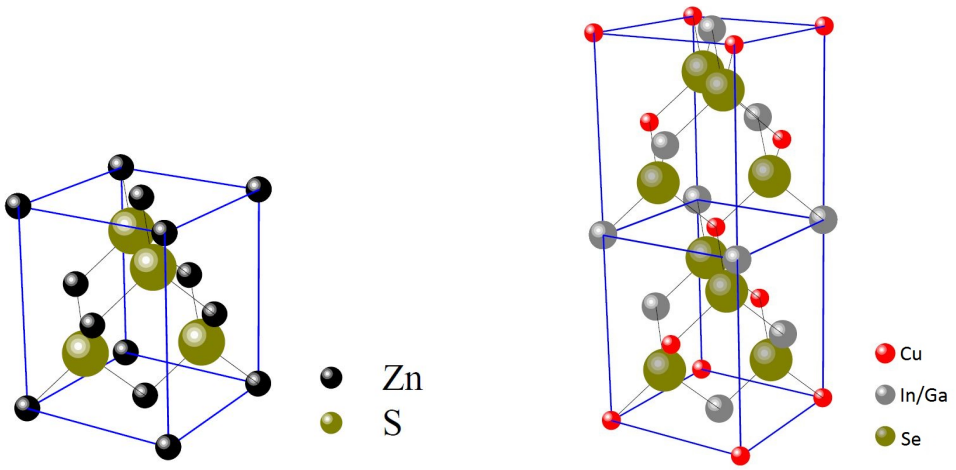

Figure 2.1: Crystal structure of a) Zinblende and b) the chalcopyrite CIGS. Presence of various point defects lead to a partially distorted crystal structure [56].

The CIGS complex can have several defects such as vacancy defects (copper vacancy (V_{Cu}), selenium vacancy (V_{Se}) or indium vacancy (V_{In})), anti-site defects (In_{Cu}, Cu_{In} etc.) and interstitial defects (Cu_i, In_i etc.) [51]. Understanding the nature of such native defects (donor or acceptor like) in a CIGS device is important given their large number and role as recombination centres (deep and shallow). Furthermore, the defects are responsible for certain unusual device properties shown by the material: 1) intrinsic doping by native defects, 2) large structural tolerance to off-stoichiometric growth and 3) benign nature of certain structural defects. The probability of occurrence of these defects depends on their defect formation enthalpies. For instance, Zhang et al. [69] found that energy needed to create V_{Cu} defects in Cu-poor or near stoichiometric material was very low; even negative formation energies have been predicted implying that the defect formation is spontaneous under equilibrium conditions. The p-type nature of the CIGS semiconductor is attributed to this shallow acceptor level V_{Cu}, often in the order of $10^{16}cm^{-3}$ [50]. Double donor anti-site defect In_{Cu} and selenium vacancy defects (V_{Se}) act as compensating donors (Figure 2.2). Donor-acceptor like defect pairs like ($2V_{Cu}^{-}$+Ga_{Cu}^{2+}) and ($2V_{Cu}^{-}$+In_{Cu}^{2+}) also have low formation enthalpies and are electrically benign in nature [50]. The tolerance towards non-stoichiometric composition can be ascribed to the highly compensating nature such donor-acceptor like complexes which are able to passivate large defect concentrations.

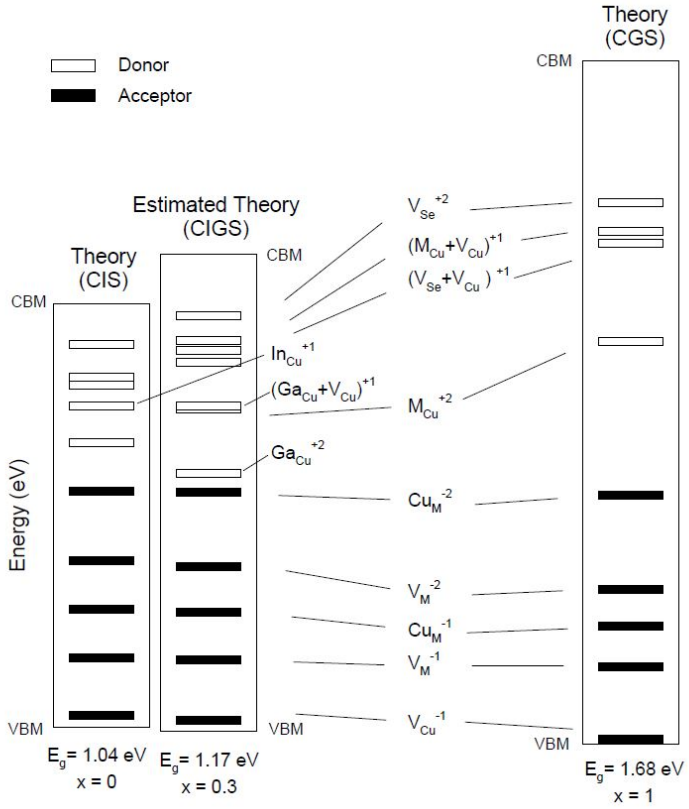

Figure 2.2: Various defects in a CIGS semiconductor and their relative position in the band gap of the device [50].

Inclusion of alkali metals like sodium, potassium, rubidium etc. have shown to improve the electrical performance of a CIGS absorber. They can be added directly into the absorber via a pre-deposition treatment (like spin coating) or diffuse into the absorber through a suitable substrate. The explanations for their positive impact on cell performance are many and are still being studied. Sodium for example, diffuses into the bulk from the soda lime glass (SLG) during the CIGS deposition process. Studies have shown that limited amounts of sodium in the absorber improves cell morphology, increases p-type conductivity and changes the defect distribution in the absorber [39, 50, 51]. Some of the many reasons provided in literature for the above occurrence include: 1) Na substitutes In and/or Ga in In_{Cu} and/or Ga_{Cu} donor like anti-site defects to form neutral complexes, thereby reducing the compensating donor concentration [4] and 2) Na substitution leads to creation of intrinsic defects: NaIn and/or NaGa which act as acceptors [41] 3) creation of $NaSe_x$ reduces the growth of $CuInSe_2$ and assists in the incorporation of Se into the film [32]. Still, it must be noted that the observations and predictions presented here explain only a part of the effects of Na incorporation. Further investigation is being carried out to understand the role of alkali metals in more details.

By varying the amount of copper in CIGS bulk, a wide compositional range of the “copper poor” ([Cu]/[In+Ga] <1) and "copper rich" ([Cu]/[In+Ga] >1) absorbers can be obtained, with the stoichiometric composition being 1. Cu-rich CIGS devices are fabricated when grown under Cu-excess conditions. Under such deposition conditions, Cu_xSe phases are formed either on the surface or the bulk of the absorber [56]. The term “copper rich” refers to this additional Cu_xSe secondary phase along with the averaged composition containing stoichiometric chalcopyrite. Staying close to the stoichiometry minimizes the defect density and improves crystal quality (grain size improves as Cu content increases). However, for Cu-rich CIGS absorbers, higher interface recombination and lower shunt resistance have been reported by many groups [21, 64]. The absence of ordered defect compounds (ODC, buried junction) at the surface of Cu-rich absorbers leads to increased surface recombination while the formation of overly conductive secondary phases (Cu_xSe) heavily shunts the device functioning. Thus, it is common practice in the industry to use slightly copper poor and selenium rich CIGS absorbers. High efficiency solar cells are obtained for Cu content typically in the range of 22% to 24% [7].

2.2. Thin-CIGS solar cells- Issues and challenges

The critical issue for a thin-CIGS absorber is that the thickness is similar to or below its optical length (<500 nm) leading to incomplete light absorption and increased interface recombination losses (increased surface to volume ratio). Recombination losses are caused due to the presence of open dangling bonds via defect states within the bulk CIGS (bulk recombination) or at the interface region of two different material layers (interface/surface recombination). The defect states can be created due to i) manufacturing defects such as diffusion of detrimental elements like Cr, Mg, Fe during high temperature absorber deposition processes (>530°C) ii) naturally grown defects due to the creation of grain boundaries in the poly-crystalline absorber and iii) undesirable secondary phases related defects ($CuSe_2$ or $MoSe_2$) [28]. Regions of the cell where such recombination occurs are known as recombination centres or trap states. In these regions, the photo-generated charge carriers get “trapped” by the dangling bonds, preventing them from getting collected at the cell contacts. Interface recombination losses (Mo/CIGS) are more dominant than the bulk due to a higher surface to volume ratio, caused by the reduction in the absorber thickness. Furthermore, the space charge region (SCR), where electron-hole pairs are separated, is very close to the interface regions of the cell (Mo/CIGS and CIGS/CdS). This leads to increased interface recombination which reduces the probability of carrier collection. In a polycrystalline CIGS absorber, the recombination rate (R_H) (governed by the Shockley-Read-Hall recombination process) is directly related to

density of trap states (N_{it}) and charge carrier concentration (n or p). Charge carrier life time τ, the time before which the generated photo-carrier gets collected is affected negatively with increased recombination. τ is inversely proportional to v_{th} or the surface recombination velocity, a parameter used to quantify the surface recombination loss: higher the v_{th}, higher the surface recombination losses. For the highly recombinative interfaces of the CIGS absorber, the v_{th} can be as high as 10^5 cm/s.

2.3. State of the Art research

Several research groups have explored novel strategies to reduce the defects in the interface region and improve light absorption including: improved back contact, rear surface passivation and gallium (Ga) grading in the absorber.

2.3.1. Gallium grading

Within the bulk of the CIGS absorber, it is beneficial to have a slightly higher concentration of gallium near the interface regions of the cell. This variation of gallium at different depths of the absorber is known as gallium grading (expressed by the GGI ratio (GGI=Ga/Ga+In)). As explained elsewhere, increasing the gallium content changes the bandgap of the material (from 1.04 to 1.68 eV), with change only influencing the conduction band alignment (w.r.t vacuum level) of the band gap. At the rear interface, this gradient induces a quasi-electrical rear surface field which aids in the collection of photo-generated electrons by repelling the electrons away from the surface. This reduces the chances of the minority charge carriers being "caught" by trap states or recombination centres, enhancing the V_{OC} of the cell (Figure 2.3). Thus, to suppress the carrier recombination at the interface regions of the cell, the GGI ratio is monotonically increased in a graded-CIGS solar cell. Wei et al. [63] theoretically (computer simulations) showed that the band-gap widening (rise in the V_{OC}) was because of the rise in conduction band offset, which increased as the GGI content increased from 0 to 1 (up to 0.6 eV). In support to his work, Kotipalli et al. [28] reported that increasing the GGI ratio from 0 to 1 increased the V_{OC} by 25 mV, when compared to an ungraded reference CIGS solar cell. This increase was attributed to a reduced interface and SCR region recombination. Furthermore, he also reported a marginal improvement in the J_{SC} due to the added drift field created by varying the GGI ratio (close to the Mo surface).

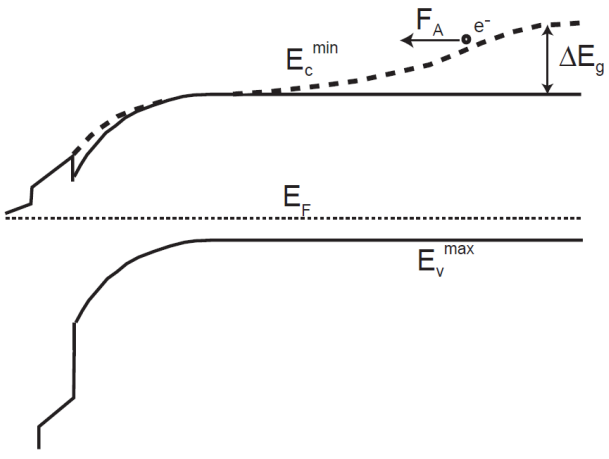

Figure 2.3: A illustration of Ga grading in the rear surface of a CIGS solar cell [34].

Efficiency improvements have also been reported, with an increase from 20.8% to 21.7% being reported by Chirilă et al. [2] due to optimized front Ga grading and better interface quality.

As for the front interface, the CdS/CIGS interface region would benefit from the decoupling of photo-generation and carrier recombination. Thus, the gallium grading induces a pseudo-passivating effect in the CIGS device which improves cell performance. However, the control and consistency of the GGI ratio in the cell is an issue, experienced by all the above authors. The long-term stability of a gallium graded CIGS device is a concern and now under extensive study. Szaniawski et al. [59] for example, showed that abnormal levels of gallium (GGI>0.3) introduced new defects in the bulk absorber, as Ga is itself an impurity. This effects the mobility of generated charge carriers as they are trapped by the additional defects states created by gallium in that region. In conclusion, a controlled amount of gallium content in the cell is necessary for reducing recombination losses, but the adverse side-effects need to be reduced. Thus, other controllable and predictable methods of introducing gallium into the cell should be investigated.

2.3.2. Back contact: Poor reflectance

For thin CIGS absorber layers (<500 nm), light in the near infra-red region of the solar spectrum is absorbed poorly. This effects the charge carrier generation which in turn reduces the maximum current drawn from the solar cell. To give incoming light a second chance for absorption, light is reflected into the absorber by the back contact of the cell. Molybdenum is regularly used as the back contact for CIGS solar cells, distinguished by its high conductivity and thermal stability. However, after studying the opto-electrical properties and impacts of a CIGS solar cell with a Mo contact, Li-Kao et al. [33] concluded that Mo is a poor reflector of light (<60% reflectance, Figure 2.4). Furthermore, it was found that the electrical characteristics such as J_{SC} and external quantum efficiency (EQE) of the cell were affected by its poor reflectance. This claim was further substantiated by the scientific works of J. Krc et al. [31], who simulated the effects of optical losses due a Mo contact in a CIGS device and reported that there was a 15% increase in the optical losses in a thin absorber (<500 nm) when compared to a standard 2000 nm layer. This loss was attributed to the poor reflectance and higher absorption of the Mo layer. Reflecting unabsorbed light back to the absorber increases the probability of photo current generation and collection.

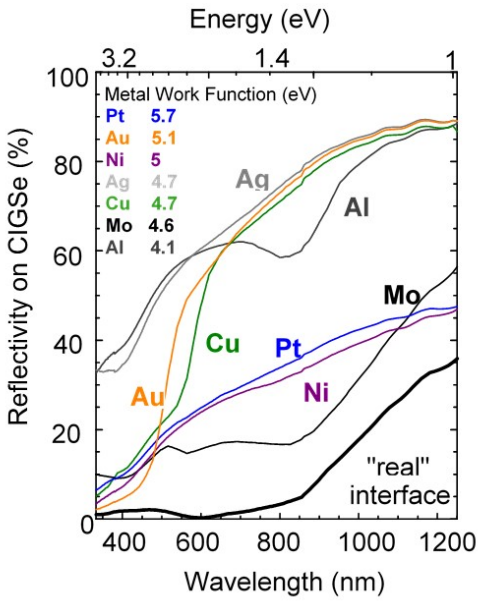

Figure 2.4: Reflectively of light as a function of wavelength into a standard CIGS absorber for different back metal contacts. Metals like Silver, Copper and Gold have superior reflectively when compared to Mo for all the wavelengths [43].

Thus, replacing the poorly reflective Mo contact by alternative materials with higher reflectance and lower absorbance have been investigated by several groups. Orgassa et al. [43] for example, identified tungsten (W) and tantalum (Ta) as possible replacements; a 0.4% absolute increase in the efficiency observed when using W for instance due to reduced absorption. Dahan et al. [5] and Z Jehl et al. [26] used highly reflective metals like gold and silver, most useful from an optical standpoint. In addition to this, Malmström et al. [35] investigated and found titanium nitride (TiN) to be an alternative back contact material as there was an enhancement of 0.8 $mAcm^{-2}$ in the photocurrent in contrast to a plain Mo contact due to an improved reflection of light in the infra-red region. When interpreting these findings though, it is essential to acknowledge the factors that impacted these outcomes. For example, gold and silver are favourable from an optical standpoint, but applies only to small area cells. Although the author did not try to explain this finding, it is plausible that the cost of the alternative materials impacted its feasibility. Also, the long-term stability of metals like W and Ta is a concern as these materials react with selenium during the absorber growth process. Hence, R. Kotipalli et al. [29] could be correct in his proposal that despite its poor reflectivity, Mo remains to be a cost-effective and stable option, with "modifying" the Mo surface (for example, using metallic nano-particles on the surface) being a more advantageous rather than completely "replacing" it with a different material.

2.3.3. Rear surface passivation

The idea to use a passivation layer for a CIGS absorber originated from the Si-PV industry where ultra-thin dielectric layers have been used extensively to passivate both p-type and n-type absorber surfaces. As explained earlier, the recombination rate can be reduced by either reducing the density of trap states (N_{it}) or by reducing the charge carrier densities (n and p). One way is to pacify the open dangling bonds present at the interface region such that, the density of recombination centres are reduced. To reduce the trap density, an ultra-thin film (<50 nm) of a dielectric material (such as Al_2O_3, SiO_2 etc.) can be used in the interface regions (in this case Mo/CIGS or CdS/CIGS). The dielectric layers pacify the interface region via lattice matching. This type of passivation is known as chemical passivation. Additionally, such dielectric materials have a fixed density of charge carriers (+ve/–ve) in its bulk. This creates a built-in electrical field which when strong enough, shield minority charge carriers from getting recombined at the interface trap states (Figure 2.5).

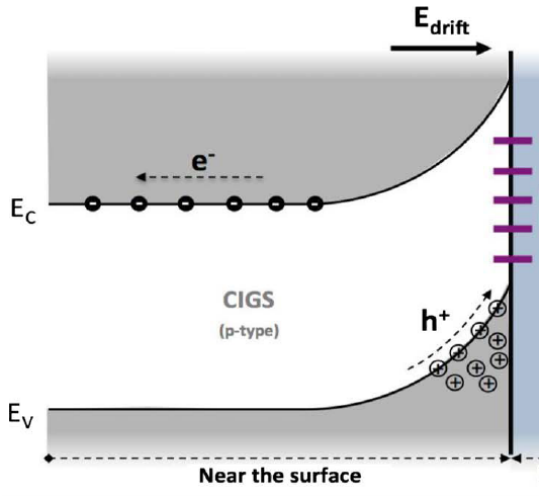

Figure 2.5: Field effect passivation in the rear interface. The stronger back surface field due to the bulk negative charge in the Al_2O_3 layer repels the minority electrons, thus reducing the rear interface recombination [30].

This passivating effect created by an electric field is known as field effect passivation (FEP). FEP reduces the concentration of charge carriers (p or n, depends on the charge composition of the passivation layer), which results to an overall reduction in the recombination rate. High efficiency (>22%) passivated emitter and rear totally diffused solar cells (PERT) were made possible due to such dielectric layers with the term "passivated" being a direct reference to passivation schemes used in these cells. More than 10% of the c-Si solar cells in the PV market now unitize passivation layers in their interface regions, proving the potential and importance of such layers. CIGS absorbers, being poly-crystalline, have defect states at the interface region that are orders of magnitude higher when compared to mono-crystalline Si absorbers. Hence the issue of rear-interface recombination losses in such absorbers is severe. Learning from the c-Si technology, passivation layer schemes are now being implemented for thin-CIGS solar cells. The advantages of field effect passivation were highlighted M. Gloeckler et al. [11] who inserted an electron passivating layer in a 500 nm CIGS cell to improve the V_{OC} by 100 mV when compared to a plain reference device. The effects of rear surface passivation with localized point contacts were studied by B. Vermang et al. [61] who showed that for a 400 nm thin CIGS absorber with a 5 nm aluminium oxide passivation layer, the J_{SC} and V_{OC} improved by 7.9 mA/cm^2 and 57 mV respectively when compared to a reference sample. Comparable results were reported by W.Ohm et al. [42], who used a porous Al_2O_3 layer to passivate the rear surface interface (SnO_2: F/CIGS (620 nm thick)) and obtained higher short-circuit currents (+1.5 mA/cm^2) and open-voltages (+37 mV) when compared to standard plain Mo sample. Remarkably, E. Jarzembowski et al. [25] from his experimental studies on a thin-CIGS solar device, deduced that the rear-surface recombination only had a minimal impact on the cell performance. He suggested that the decrease in cell performance due to thinner absorber layers was better attributed to incomplete absorption of light. He substantiated this claim by using a back reflector made of nano-structured SiO_2 coated on the Mo surface to improve the cell efficiency by roughly 50% for a 190 nm thick CIGS absorber layer [25].

2.3.4. Aluminium oxide passivation schemes

For passivation, the choice of the dielectric material depends on several parameters such as the interface passivation quality, thermal stability, industrial viability, surface adhesion properties, deposition temperature and optical absorption/reflection. In c-Si technology, thermally grown SiO_2 films have been used as they offer excellent surface passivation qualities (surface recombination velocity <30 cm/s) and reduce parasitic junction formation beneath the silicon surface. However, its industrial viability was a concern due to its high temperature deposition requirement. The high temperature deposition also tends to degrade the bulk lifetime of the silicon cell. Next, extensive research was carried out on silicon nitride, which were deposited at temperatures below 400°C. However, the silicon nitride (SiN_x) passivated cell had a reduced V_{OC} and FF when compared SiO_2 passivated cell. This was attributed to the fixed density of positive charge in the bulk SiN_x which created an inversion layer at the p-type silicon surface. It induced a floating junction which lead to parasitic shunting with the rear contact of the device. This resulted to the introduction of an aluminium oxide layer, which 1) has a fixed density of negative charge in the bulk and 2) can be deposited at temperatures of less than 200°C. Its excellent passivation qualities have been proven in both p-type and n-type silicon surfaces; the v_{th} was brought down to 5 cm/s. This is generally ascribed to the high concentration of fixed negative charge (10^{13} cm^{-2}) in its bulk and reduced trap density at the Si-Al_2O_3 interface (10^{12} eV^{-1}cm^{-2}) [62]. Thus, owing to its sound passivating qualities and as an alternative for Ga grading, Al_2O_3 passivation layers are now being implemented in thin-CIGS devices to reduce the interface recombination losses. Having similar recombination mechanisms (SRH for both), the same approach could be applied to reduce the charge carrier interface recombination which would then improve the electrical performance of a thin-CIGS absorber.

As the passivation layer (Al_2O_3) is needed at the CIGS/Mo interface, it must be deposited post-Mo sputtering and pre-CIGS deposition. Al_2O_3 being a thermally stable compound, can withstand the high temperature (550°C) and highly corrosive (Se gas) absorber deposition process. This is one of the many reasons to choose Al_2O_3. Accordingly, W.-W. Hsu et al. [22] performed the first characterization studies on CIGS solar cells with Al_2O_3 rear surface passivation schemes. Using photoluminance (PL) measurements he showed that, for a Mo/Al_2O_3/CIGS cell stack, the PL peak was amplified by a factor of 100 when compared to a reference Mo/CIGS sample (Figure 2.6). The intensity of a PL spectrum is reduced when non-radiative recombination losses increases.

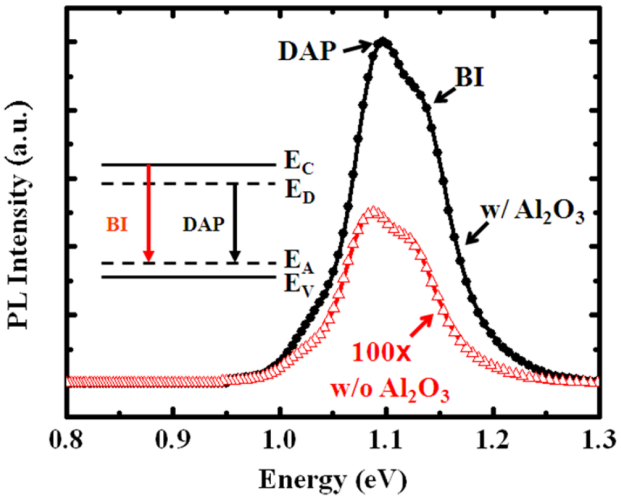

Figure 2.6: The spectral intensity peaks for CIGS cells with and without a rear-passivation layer [22]. An increase in spectral intensity can be seen for passivated cells, especially in the CIGS band-gap region (1.0-1.2 eV).

This suggests that the band-impurity and non-radiative recombination were reduced for cells with the interface passivation. Furthermore, he reported that for a 50 nm Al_2O_3 passivation layer, the defect density (N_{it}) could be reduced by up to 35% when compared to unpassivated cells. This would imply that Al_2O_3 is an excellent chemical passivating layer for the rear surface of the cell. Such reductions would lead to low surface recombination velocities close to 100 cm/s (from 10^5), paving way for reduced absorber thicknesses without efficiency losses. Likewise, R. Kotipalli et al. [29] performed advanced opto-electrical characterizations on a Mo/22.5 nm-Al_2O_3/CIGS cell to quantify the field effect and chemical passivating effect of the Al_2O_3 passivation layers. From those measurements, he calculated the fixed negative charge density and interface trap density to be (10^{13} cm^{-2}) and ($10^{11} eV^{-1} cm^{-2}$) respectively. Furthermore, computer simulation models were made to visualize the effects of an aluminium oxide passivation layer (rear surface). The effects of field effect passivation were clearly observed; a reduction in the minority charge carrier concentration by two orders of magnitude was reported when compared to an un-passivated sample. This can be explained as follows; a high density of negative charge in the bulk Al_2O_3 causes the conduction and valance band to bend upwards, creating a built-in electric field which deters the collection of minority charge carriers in the rear interface. Interestingly, the field effect passivation is only activated after a post-deposition annealing (PDA) step as the as-deposited Al_2O_3(AD) layer exhibits a fixed positive charge density (at the rear contact, holes are collected and electrons need to be repelled off the surface). This annealing step is however not essential for a CIGS cell as the high temperature absorber deposition process is itself sufficient enough to activate the Al_2O_3 layer.

2.4. Deposition Techniques

To integrate an aluminium oxide passivation layer in the CIGS device, a thin-film deposition method is needed that is controllable, gives good conformity, uniformity and has excellent step coverage for the layer deposited. Many thin-film deposition techniques like sputtering, chemical vapor deposition (CVD) and atomic layer deposition (ALD) can be used for Al_2O_3 deposition. However, for deposition techniques like sputtering and CVD, the film growth rate depends on the flux of growth species and the duration of deposition process. This makes it difficult and challenging to deposit high quality ultra-thin films (<100 nm) when the deposition rates are high. Additionally, in non-planer surfaces, objects that are not in the direct-line of sight with the flux source experience reduced or even zero growth rate (Figure 2.7). Unavoidably, complex 3D structures like trenches, fins and nano-particles are coated non-conformally. This affects the uniformity of the layer coated [47]. Furthermore, for uniform layers over large area substrates, uniform growth flux is necessary with respect to the full substrate area which is difficult to control. Given the many limitations of the aforementioned deposition techniques, atomic layer deposition (ALD) was chosen for the current research work. Moreover, this was the only tool available for Al_2O_3 deposition at IMEC, hence there not much flexibility in this aspect.

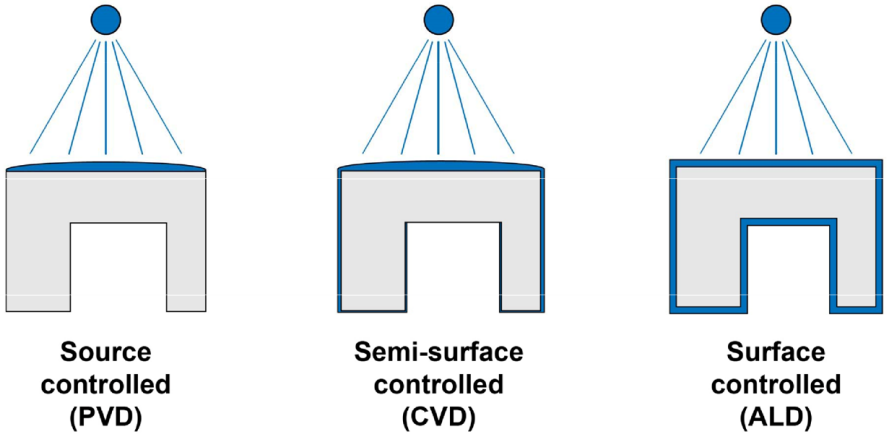

Figure 2.7: A diagram depicting the self-limiting, conformal and uniform growth in ALD depositions when compared to other deposition techniques [47].

2.4.1. Atomic layer deposition

ALD is vapour phase deposition method in which thin films are generated by repeating two chronologically executed half-cycle reactions. The duration of the half-cycle depends the time taken by the precursor vapour to completely react with the functional groups of the substrate. Ideally, these reactions are self-terminating in nature i.e. the precursor material is un-reactive to the functional groups formed by itself and ceases to continue if all the surface groups have reacted. This leaves only a monolayer film on the substrate surface after the completion of one complete ALD cycle. Usually, inert gas like Argon or Nitrogen are used to remove any un-reacted precursor and other volatile reaction by-products from the reactor chamber. Despite the many advantages of ALD, it still faces two critical shortcomings which restricts its large scale industrial use. The first is the slow deposition rates (50 nm/hr) or growth per cycle for conventional ALD - up to 2 orders slower when compared to chemical vapour deposition. This drawback is a consequence of the unique advantage that ALD provides, i.e., the self-limiting nature of reactions in ALD. As the substrate is exposed to a sequence of purging and pulsing steps to deposit the film, the time taken for each of these individual steps contribute to the overall delay of the process when compared to other deposition techniques like CVD and sputtering.

Secondly atomic layer depositions usually involve vacuum processing making it difficult and uneconomical to scale up. These drawbacks were however mitigated by the recent development of a faster and simpler deposition technique called Spatial ALD. This was achieved by splitting up the reaction precursors spatially. Thus, the different precursors are supplied uninterruptedly but in different physical locations (Figure 2.8). Consequently, there are at least two regions in the spatial ALD setup where the half reactions occur on the sample. This method has become prevalent in the recent years due to its conceptual ease.

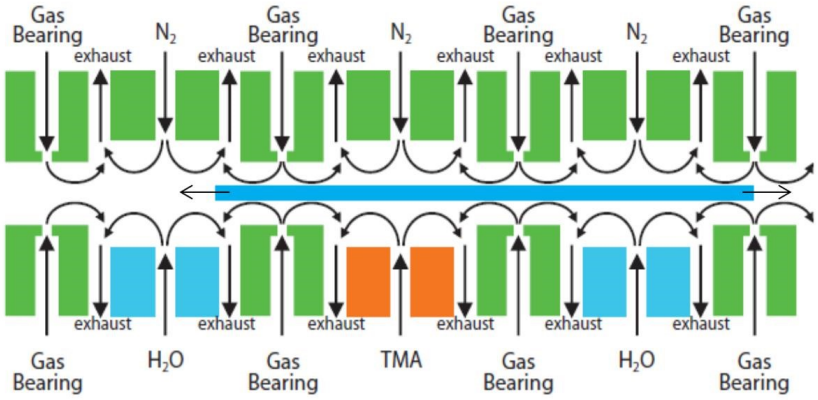

Figure 2.8: Graphical illustration of Spatial ALD where the substrate moves relative to the injectors enabling a faster deposition of the thin film [38]. This method makes ALD industrially viable due to its high deposition rates.

By maintaining the substrate in a half reaction zone for a given time interval, an ALD monolayer can be grown from the first precursor. The substrate is then moved to the second half reaction zone, where another ALD cycle is completed to form a monolayer. Alternately, the substrate position can be fixed, and the precursor injector heads can also be moved to the position over the substrate, or a combination of the two can also be used. It does not require vacuum and can be easily performed at ambient temperatures [38]. Thicker deposition layers can be obtained by repeating the above steps for desired number of cycles. This allows for quicker deposition rates (3600 nm/hr), only limited by the precursor reaction kinetics i.e. time needed for a complete reaction to take place when the substrate is in the precursor zone. The main characteristic of ALD lies in the decoupling of the two independent half reactions which requires a complete segregation of the precursors. In conventional ALD it is achieved using purge steps in between the precursor pulse steps. In spatial ALD, the half reactions intermixing is prevented by implementing a combination of physical barriers and continuously flowing precursor streams. Summarizing, the three main characteristics of spatial ALD are: (1) physically separated half-reactions zone, (2) movement of the precursor injector heads and/or the substrate, and (3) a barrier between the half-reaction zones to prevent intermixing of the different precursors.

3

Fabrication Steps and Electrical Characterization

3.1. Device Fabrication

In this thesis, the CIGS solar cells were fabricated in the steps illustrated in Figure 3.1. A substrate configuration was used for cell fabrication.

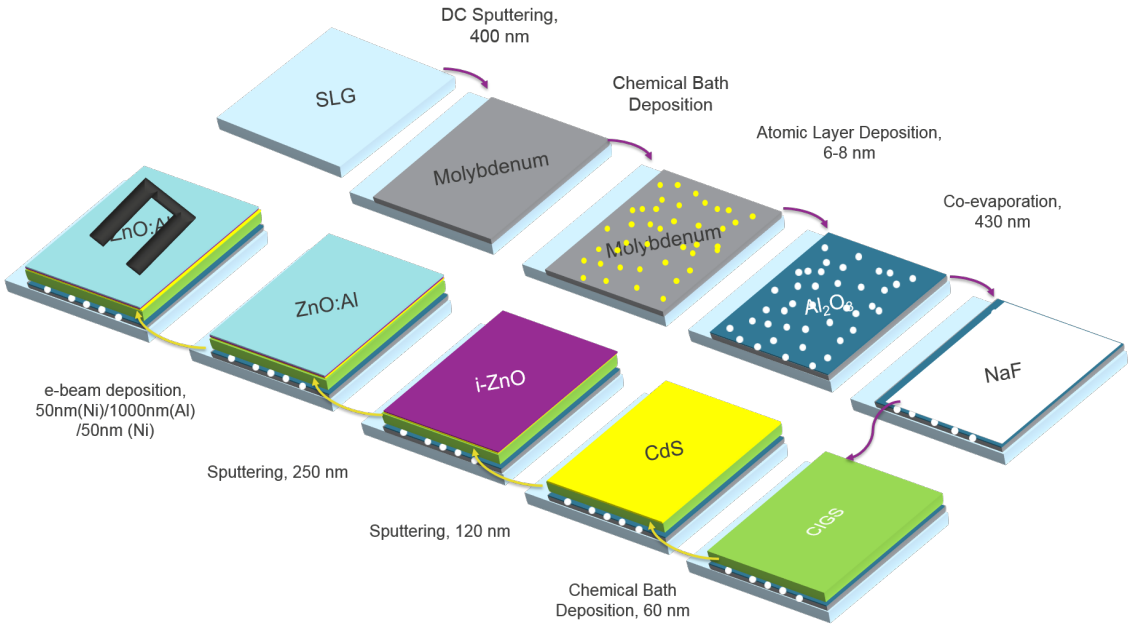

Figure 3.1: The various steps involved in the fabrication of a passivated thin-film CIGS device. A 1-stage co-evaporation process is used for the absorber deposition.

3.1.1. Glass substrate

A standard 3 mm thick soda lime glass substrate was used for all the fabricated devices. SLG is used due to its lower cost (3 €m^{-2} in 2015), stability at higher temperatures of up to 550°C, as a source of sodium and for its thermal expansion of 9.5 ppm/K (close to that of molybdenum and CIGS). However, flexible substrates based on polyimides or ultra-thin glass can also be used. Furthermore, at IMEC, the SLG glass is available with an alkali barrier layer and a pre-deposited layer of molybdenum (around 400 nm) on one side. Mo is used as it has an electron affinity of about 4.5 eV which

allows for the formation of an ohmic contact with the CIGS bulk (partly due to the formation of a $MoSe_2$ layer). Moreover, the Mo layer also has good surface adhesion with the CIGS layer and is permeable to alkali metal diffusion (for example, diffusion of Na between the Mo grains). The substrates are available as big 30 cm × 30 cm pieces, thus, a diamond-tip cutting tool is used to size the glass substrates into smaller pieces of 5 cm × 5 cm. To remove any oxide or organic waste layers from the Mo surface, the substrates are cleaned in 30 wt.% ammonium hydroxide (NH_4OH) solution for about 5-6 minutes. This is followed by dipping the substrate in clean water and isopropyl alcohol (IPA) for 3 minutes each. The water is used to wash away any excess NH_4OH from the substrate surface while the IPA is used to wash away any excess water from the substrate surface. The substrate is then dried with an N_2 gun.

3.1.2. ALD for Al_2O_3

The Al_2O_3 depositions were performed in a temporal-ALD system (Cambridge NanoTech). The depositions were performed using tri-methyl-aluminium (TMA) as the precursor vapour which is pulsed (usually 10-16 ms) in the first half of the reaction cycle. It reacts with the hydroxyl groups present on the substrate (Mo in this case) to produce methane as the reaction by-product. A purge step (typically around 20-30 seconds) is used to remove excess TMA and methane. Subsequently, H_2O is pulsed (usually 30 ms) in the second half of the reaction cycle. Here, the dangling methyl groups from the previous cycle react with the H_2O to form aluminium oxygen bridges with methane as a by-product. Another purge strep removes the reaction by-products to complete the reaction cycle, shown in Figure 3.2. The thickness of the film coated depends on the growth per cycle or GPC (found to be 0.12 nm/cycle, thickness found using ellipsometry measurements) i.e. one complete cycles grows a layer of certain thickness thus, more the number of cycles, greater the thickness of the layer deposited. Since both the half-cycle reactions are self-limiting, using ALD depositions, sub-nanometre resolution of film growth can be achieved provided that the pulsing and purging steps are sufficiently long (until the surface reaction saturates).

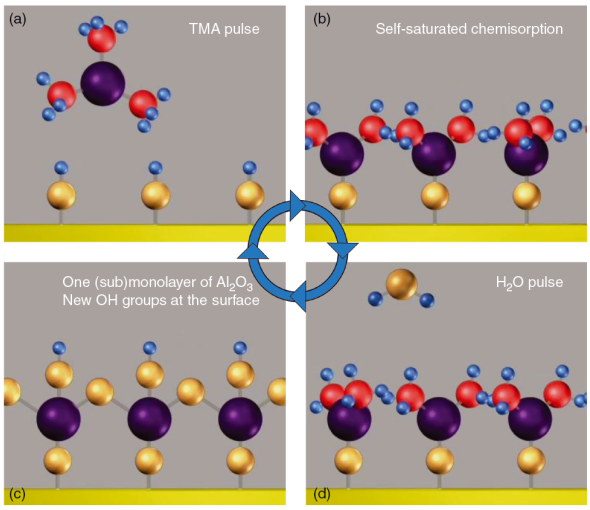

Figure 3.2: A pictorial depiction of an atomic layer deposition for Al_2O_3. The four different steps (two pulsing cycles (TMA and H_2O) and purging steps) and their self-limiting nature is seen from the above illustration.

3.1.3. CIGS deposition

The CIGS absorber was deposited using a single-stage co-evaporation process. In this process, the precursor elements namely copper, indium, gallium and selenium are all evaporated from their re-

spective sources on to the substrate at set individual temperatures; 1300°C for Cu, 1000°C for In and 1050°C for Ga. To begin with, the substrate is initially heated to a temperature of 550°C under a selenium environment. Next, the copper, indium and gallium precursors are co-evaporated for about 30 minutes. After the precursor deposition, the substrate is annealed in a selenium environment for another 10 minutes. At the end, the substrate is cooled down again in a selenium environment for a few more minutes to end the deposition process. Since the sticking coefficients of the metal precursors are high, the final film composition and growth rate can be found by the effusion rate and flux distribution of each source. Thus, to calibrate the system, a dry run is done before the actual deposition. Figure 3.3 depicts the 1-stage co-evaporation process used for this thesis. XRF measurements were taken (36 measurements on a 10 cm by 10 cm substrate) to find the thickness and composition of the deposited film. In the present work, the CGI ratio was about 0.7 ±0.01 while the GGI ratio was 0.29 ±0.01 for a 430 ±10 nm layer.

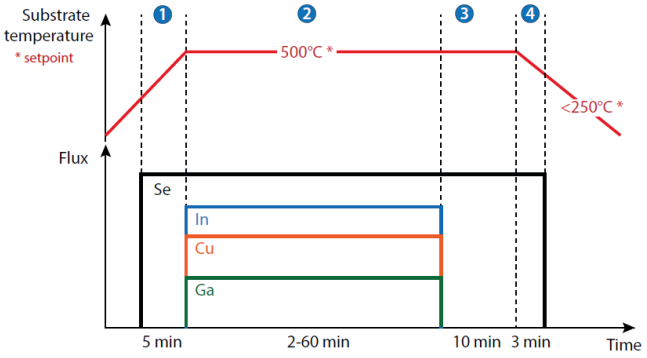

Figure 3.3: An illustration of a 1-stage co-evaporation process [37].

3.1.4. Buffer layer, CdS

An n-type cadmium sulphide (CdS) buffer layer forms a heterojunction with the CIGS layer. The CdS film (50 nm) was made using a chemical bath deposition process. For this, the substrates were held in a solution containing cadmium acetate and thiourea at 65°C for a certain time (to allow the CdS film to grow). The toxicity of cadmium is a concern and research is also being carried out at IMEC to look for alternative buffer layers. However, this is not the objective of the current thesis work.

3.1.5. Transparent conductive oxide

A good TCO layer should have a balance between being transparent to incoming solar spectrum and being conductive to reduce resistive losses. For electron conduction, a TCO layer consisting of a 120 nm layer of intrinsic-zinc oxide and 250 nm of aluminium doped zinc oxide was sputtered on the buffer. This layer reduces shunt paths in the CIGS device due to its high resistivity [58]. Low refractive index materials (ex. MgF_2) can be used as an anti-reflection coating however, none were used in this research.

3.1.6. Front and back contacts

For the front contact, a Nickel (50 nm)/Aluminium (1 μm)/Nickel (50 nm) was deposited using e-beam evaporation. For the back contact, on any one end of the device all the layers (except the Mo layer) are scribed away (using a needle) and indium in soldered onto the molybdenum. A mechanized blade was then used to scribe the surface of the device to generate cells (0.5 cm^2).

3.2. Electrical Characterization

3.2.1. Current density and Voltage (J-V)

Solar cells are diodes generating photo-current under forward bias conditions. To study the diode characteristics of a solar cell and measure important electrical parameters such as J_{SC}, V_{OC} and maximum power generated, J-V measurements are essential. A WACOM solar simulator system was used to generate an AM1.5 spectrum while a 2401 Keithley source meter was used to acquire and measure the J-V characteristics. The intensity of the solar spectrum was pre-calibrated to mimic the AM1.5 spectra. All the experiments were performed by keeping the device at a temperature of 25°C unless specified specifically. To reduce the effects of heating (by the solar simulator), a shutter was used in between successive measurements.

3.2.2. External Quantum Efficiency

The external quantum efficiency of a solar cell is a measure of how effective the solar cell is in collecting the charge carriers from photons of a certain energy incident on its surface. The EQE depends on the probability of carrier collection and light absorption. Thus, high recombination losses lead to loss of generated carriers which effects the EQE spectra. An in-house system using a xenon-lamp and grating monochromator was used to measure the EQE spectra in this work.

3.2.3. Capacitance-Voltage Measurements

By applying a range of voltages over the solar cell and measuring the corresponding capacitance, the depletion width and majority carrier density (at the depletion edge) can be estimated. For simplicity, a one-sided abrupt junction and uniform doping are considered. An Agilent 4980A LCR system was used to perform the C-V measurements for a frequency range of 1 Kilohertz to 1 Megahertz and bias voltage varying from -2 V to 0.5 V.

3.2.4. Photoluminescence analysis

In a photoluminescence experiment, a pulsed light source is used to excite the electrons of a semiconductor material. By analysing the obtained spectra, the dominant wavelength and intensity of emissions can be found. This is done by detecting the luminescence of the electron-hole radiative recombination. In an ideal case, the energy of the dominant radiative recombination path should be the bandgap of the material . Multiple peaks or broader PL spectra suggests that more than one recombination paths exist in the semiconductor material. Excited charge carriers eventually recombine, hence greater the intensity of the PL curve, lower the non-radiative recombination in the semiconductor. This is a favourable property for a semiconductor used as a solar cell. To obtain the minority charge carrier lifetime, the photoluminescence measurement is performed as a function of time. Such an experiment is known as time-resolved photoluminescence (TRPL) measurement. In this thesis, a Hamamatsu C12132 was used for the PL and TRPL measurement. The excitation laser is Nd:YAG class 3B laser with a 15 Kilohertz repetition rate for a 1 ns pulse length. The laser has an excitation wavelength of 532 nm and a beam spot diameter of 3 mm. The optical settings of the IRIS and filters were unchanged when time-resolved photoluminescence responses were measured for comparison studies between reference devices and passivated devices. In a semi-log plot, the time constant of the fast recombination region of the plot is obtained from a 1st order fit while the minority carrier lifetime is the constant obtained from a 2nd order exponential equation. This inference is still debatable for thin-film materials like CIGS and kesterites.

4

Al_2O_3 passivated CIGS devices

Recently, high efficiencies of about 22.9% were obtained for small-area (0.5 cm^2) CIGS solar cells, however they were achieved with absorbers thicker than 1 μm. When compared to a standard CIGS absorber (2-3 μm), a thinner absorber (<1 μm) would limit usage of critical feed-stock (reduced manufacturing costs), reduce the bulk defect (due to reduced bulk volume) and increase the potential for higher manufacturing throughput (reduced deposition times). Reduced manufacturing costs for example can bring down PV production costs from 0.4 \$/W_P to 0.25 \$/W_P (for a production capacity of about 2 GW) [45]. Yet, for thicknesses lesser than 1 micrometre, the cell efficiency reduces due to the highly recombinative rear interface (the electron-hole pair generated in the vicinity of the back contact, back recombination) and incomplete absorption of incident solar spectrum (partly due to poor reflection at the rear interface). The joint effects of the same lead to a reduced V_{OC} (high rear surface recombination velocity of around 10^5 cm/sec) and J_{SC} (internal reflection of solar spectrum is below 60%) causing a reduction in cell efficiency. One approach to reduce the rear interface recombination for instance would be to use a passivation layer; the passivation layer reduces the interface recombination by field effect and chemical passivation. This work reports the implementation of one such passivation scheme namely aluminium oxide, to improve the open circuit voltage of the cell by reducing the rear interface recombination and thereby increase the efficiency for 430 nm thin CIGS absorber.

4.1. Optimization Studies

Since the passivation layer is of non-conducting type, point contacts are necessary for electrical connection. The minority carrier diffusion length limits the size and pitch (distance between the contacts) of the point contacts. When compared to c-Si solar cells (several hundred micrometres), CIGS has a very small minority carrier diffusion length and thereby lifetime. Thus, if a diffusion length of 0.5-1.25 μm is possible, nano-sized openings (a few hundred nanometres in diameter) for a pitch varying from 1.25 to 2.5 μm (scaled from the Si-PERC design) is necessary for efficient carrier collection with the contacting area varying between 4-5% [61]. Given the size of the point contacts (nano-meter scale), cost effective ways to create nano-openings can be challenging. A technologically feasible method to create nano-point contacts is used in the present case. For this, the Al_2O_3 layer was deposited on a nano-particle rich-CdS film and next, the nano-particles were removed from the surface to create the point openings. The reason for choosing CdS nano-particles is twofold 1) CdS is used as the buffer layer in the cell, hence the same CBD solution can be used (cost saving) 2) the particle size varies from 200 nm to 500 nm, more or less the optimal size required in this case. Subsequently, a particle rich CdS solution was created using a cadmium ammonium solution (cadmium precursor and ammonia as the complexing agent) and thiourea solution (sulphur

precursor) at 64°C. The substrate was immersed into the CBD solution after X minutes of reaction time i.e. the time taken for the formation of CdS nano-particles. It was then allowed to remain in the CBD solution for Y minutes during which a CdS rich film was grown on the substrate surface. Post ALD, particle removal was done in several ways such as i) mechanical wiping ii) dil.HCl immersion and/or ultrasonic agitation. A schematic of the above process is shown in Figure 4.1. Initial experiments involved the optimization of the deposition parameters X and Y to obtain an optimal 5% coverage. Post optimization, X and Y were experimentally found to be 4 and 5 minutes respectively for a surface coverage of 4-5% and a point opening diameter being 300 ±20 nm (Figure 4.2).

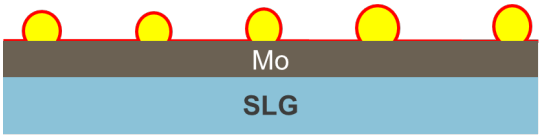

(a) CdS nano-particles (yellow) with an ultra-thin Al_2O_3 layer (red).

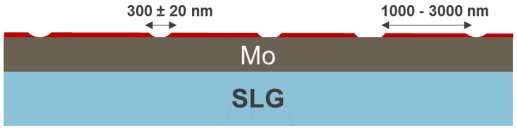

(b) Rear-interface post CdS removal

Figure 4.1: Generation of electronic contacts using CdS nano-particles for a passivated solar cell.

The thickness of the Al_2O_3 layer was also an important parameter that needed to be optimized. Ideally, thicker Al_2O_3 (>25 nm) can lead to higher rear surface reflection and stronger field effect passivation. However, for thicknesses greater than 20 nm, the Al_2O_3 surface was seen to blister during the CIGS deposition process (Figure 4.3). The blistering is a consequence of the harsh and corrosive conditions the Al_2O_3 layer must withstand; temperatures above 500°C in a selenium rich environment. At such conditions, there is extensive desorption of H_2O and H_2 gases from the Mo/CIGS interface and the bulk Al_2O_3. Al_2O_3, being an excellent gas barrier layer, traps the gases, preventing them from getting released. Consequently, cell performance is affected [61].

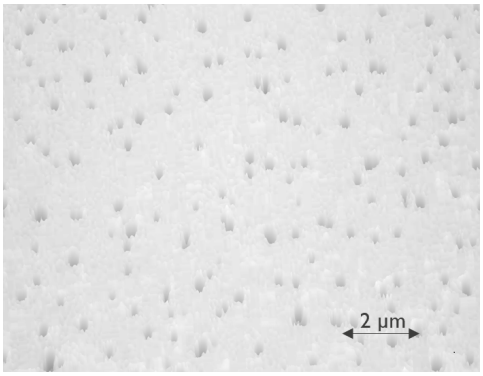

Figure 4.2: A microscopic image depicting the Al_2O_3 layer post CdS removal. The average size of the openings was 300 nm for a contact area of roughly 4.6% respectively.

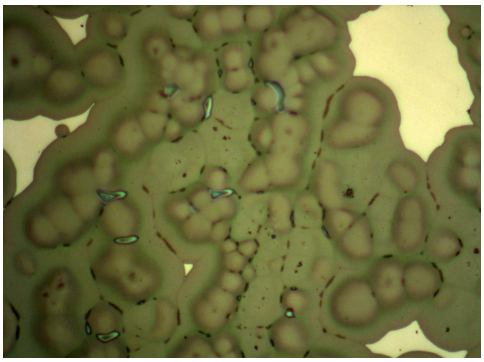

Figure 4.3: A microscopic image of blisters on the Al_2O_3 surface (25 nm). For thicker Al_2O_3 layers, the surface blisters due to the harsh absorber deposition conditions.

Hence, to avoid blistering, initially a 12 ±1 nm Al_2O_3 was used to fabricate a solar device. However, a high series resistance (about 5 Ωcm^{-2}) and low fill factor (average 55%) was obtained, indicative of inadequate contacting area. This could be due to improper particle removal (CdS buried in the Al_2O_3 layer). Consequently, the large lateral distances needed by the charge carriers to reach the point openings effects the series resistance. This is in good agreement with the results obtained by Vermang et al. [62] who showed that, for ALD deposited Al_2O_3 layers thicker than 8 nm, CdS nano-

particle removal was insufficient. The self-terminating and highly conformal ALD growth means that the CdS particles embedded in very thick Al_2O_3 layers are irremovable. Thus, an ultra-thin 6 ±1 nm layer of Al_2O_3 was used to tackle both the above issues, 1) blistering and 2) unsatisfactory particle removal. The results discussed in the next section are for the cell with the optimized deposition parameters (6 ±1 nm Al_2O_3 layer with a contacting area of about 4-5%).

4.2. Electrical Performance Results

The results presented here are for the fully optimized passivated device. The reference cell was made in the same CIGS deposition run as the passivated i.e. the Mo, CIGS and CdS layers were all deposited in the same run. For every device, 25 cells (each 0.5 cm^2) were randomly selected and electrically characterized. The statistical results for V_{OC}, FF and efficiency (η) are presented in box plots, illustrated in Figure 4.4. From the box plots, there is an improvement in the electrical performance of the passivated device when compared to the reference. For 25 randomly selected and tested cells, a 65 mV (average) improvement in the open-circuit voltage was recorded, with the highest recorded V_{OC} value being 604.4 mV for the passivated device. The reference cell had an average efficiency of 7.2% while for the passivated device it was 8.5%, an improvement of 1.3% abs.

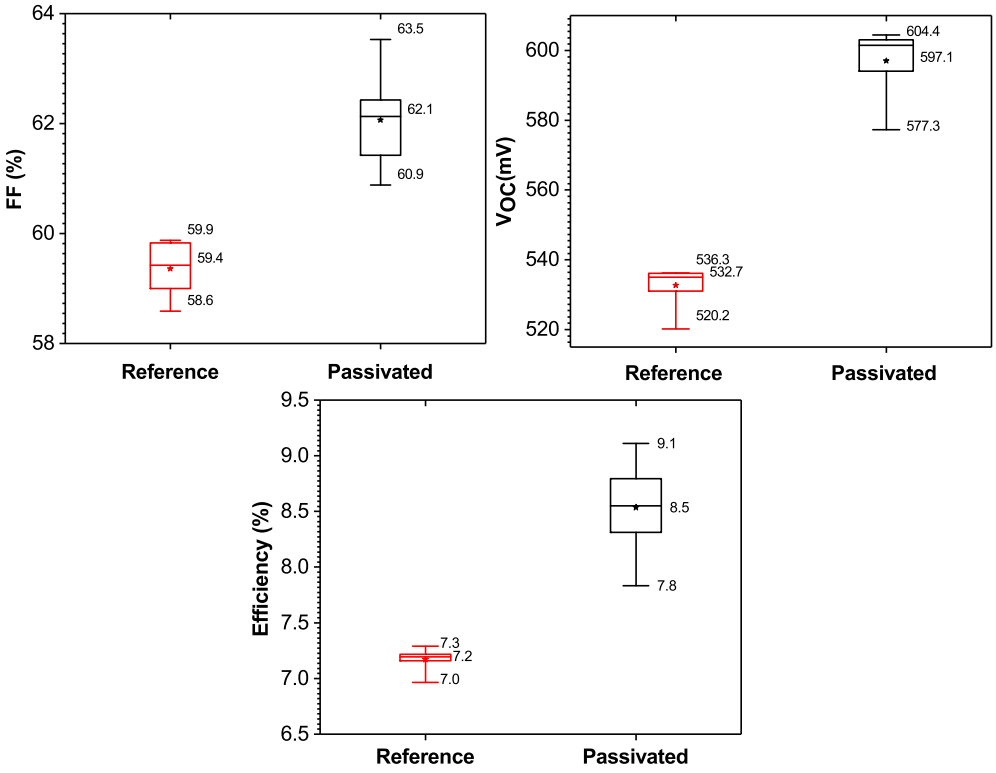

Figure 4.4: Recorded average cell efficiency, fill factor and V_{OC} for both the devices. The middle line and star within the box plot represent the median and average values of the measured electrical parameters respectively. Also, passivated cell has an optimized nano-sized local rear point contacts.

The point contacts vastly reduce the electrical contacting area in the cell, roughly to 5%. Remarkably, the fill factors for the passivated are acceptable and in fact, higher when compared to the reference cells; 62.1% for the passivated device when compared to 59.4% for the reference. Good fill factors indicate a well-defined and nearly optimized contact area in contrast to low FF values, which together with a high series resistance, is indicative of non-optimized electrical contacts.

A relatively low average series resistance of 1.3 Ωcm^{-2} (calculated using equations based on a one-diode model [19]) and high FF for the passivated device suggests that random-nano patterned Al_2O_3 layer in terms of spacing and density, creates a proper and well-defined contacting area. The low series resistance also means that the holes (majority carriers) are not hindered by the horizontal distance travelled to get collected by the nano-sized localized openings. Furthermore, for an increased open-circuit voltage, the FF is expected to improve. Equation 4.1 can be used to explain this as it correlates the FF to the open circuit voltage [13].

$$FF = \frac{v_{oc} - ln(v_{oc} + 0.72)}{v_{oc} + 1} \tag{4.1}$$

Where,
$v_{oc} = \left(\frac{qV_{OC}}{AkT}\right)$ is the normalized voltage,
A=ideality factor,
k= Boltzmann constant,
q=electron charge,
T=Temperature.

Using Equation 4.1, it was estimated that the passivated device would have a 4-6% higher fill factor when compared to the reference device. This fits well with the experimentally obtained 5% (approximate) higher fill factor for the passivated device. Now, the improvement in the efficiency can be explained by the achieved improvements in the V_{OC} (532 to 597 mV) and fill factor (59.4 to 62.1%). Sufficiently good V_{OC} (>530 mV) and decent fill factors (>59%) were obtained, however the efficiency was limited by the low J_{SC} values (< 24 $mAcm^{-2}$) in both the cases. For sufficiently good light absorption, an absorber thickness of at least 1 μm is needed [26]. However, for thin-CIGS absorbers (<500 nm) as in this case, light is insufficiently absorbed [11]. For such devices, the optical losses in the infra-red are significantly high [61]. Yet, when compared to the reference device, a 0.2 $mAcm^{-2}$ improvement in the average J_{SC} was obtained. The gain in the J_{SC} is also seen in the EQE curve (Figure 4.5, EQE of best efficiency cell in both the devices) where, the passivated cell performs better in the near infra-red region of the spectrum (550 nm-1000 nm).

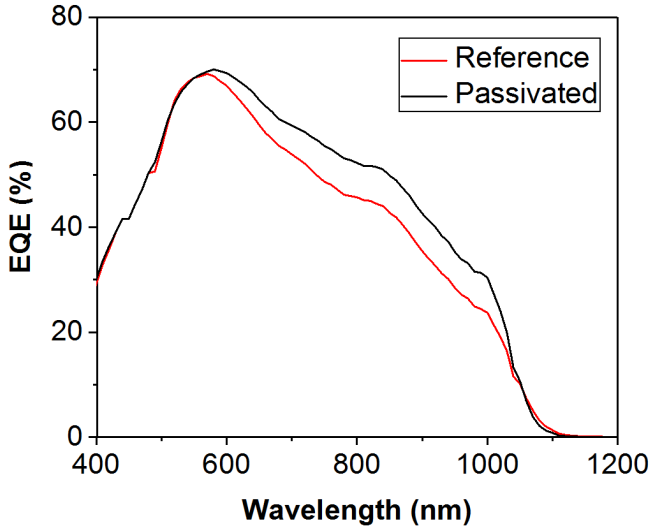

Figure 4.5: The passivated cell performs better in near infra-red region of the solar spectrum. This shows that the passivation layer improves the opto-electrical performance of the solar device.

For the passivated solar cell, a part of the light in the near infra-red region is reflected at the Al_2O_3/Mo interface into the CIGS absorber by light interference fringes. This leads to an improved current generation which is seen via the JV measurements. Also, the reflection is stronger for thicker Al_2O_3 layers, thus, only a marginal improvement in the J_{SC} was obtained in the present research (6 ±1 nm layer used) [61]. To further analyse the improvements in the V_{OC}, the forthcoming graphs will present the results of the cell with the highest efficiency in each of the device tested, presented in Table 4.1. To recap, all the devices were fabricated in the same run (average cell results were being discussed up-till now).

Table 4.1: Electrical parameters of the best efficiency passivated and reference cell.

Best cell Performance	Reference	Passivated
J_{SC} (mA/cm^2)	23.1	24.2
V_{OC} (mV)	535.1	604.4
FF (%)	59.1	62.1
Efficiency (%)	7.3	9.1

4.3. Dark JV Curve Analysis

The results of the measured J-V characteristics were analysed via MATLAB code which uses a one-diode model (Hegedus et al. [19]). An equation of the same is given below.

$$J(V) = J_{\circ}[exp\{\frac{e(V - R_{ser}J)}{AkT}\} - 1] + [\frac{V - R_{ser}J}{R_{shunt}}] - J_{SC} \tag{4.2}$$

Where,
$J_{\circ}$ = dark saturation current density,
A= ideality factor,
R_{ser} = lumped series resistance,
R_{shunt}= lumped shunt resistance.

For an ideal p-n junction, the dark saturation current density is related to the minority carrier lifetime, diffusion coefficient and charge carrier concentration given by the equation below:

$$J_0 = \frac{eD_n n_{p0}}{\sqrt{D_n \tau_b}} + \frac{eD_p p_{n0}}{\sqrt{D_p \tau_p}} \tag{4.3}$$

Where,
$D_{n/p}$ = Diffusion coefficient for electron/hole,
τ= minority charge carrier lifetime,
R_{ser} = lumped series resistance,
R_{shunt}= lumped shunt resistance.

Figure 4.6 shows representative dark JV curves for the reference and passivated device. Both the devices have good-diode like behaviour (dark JV curve) however, the reference device appeared to be slightly shunted (from the illuminated JV curve, not shown here). It must be noted that the dark JV curve for the reference cell does not show any sign of shunting; the reference cells were affected by voltage-dependent carrier collection [52].

For thin-film solar cells with shorter diffusion lengths and higher absorption coefficients like CIGS, the current generation has a larger dependence on the field assisted drift. Thus, the photocurrent is reduced by weaker fields or higher forward bias voltages. Lower diffusion lengths can be attributed to either higher bulk and/or rear interface recombination. The same is not seen for the passivated device hinting a reduced interface recombination (bulk remains the same in both the cases). A higher charge carrier life time was also obtained for the passivated device, and in the present case, the bulk remains unchanged. Hence it is attributed to passivating qualities of the Al_2O_3 layer. Now, to explain the observed improvement in the V_{OC}, the following three parameters will be used: 1) higher shunt resistance (from the dark JV curve) 2) reduced dark saturation current density (from the dark JV curve) or charge carrier recombination and 3) majority charge carrier concentration (holes in this case).

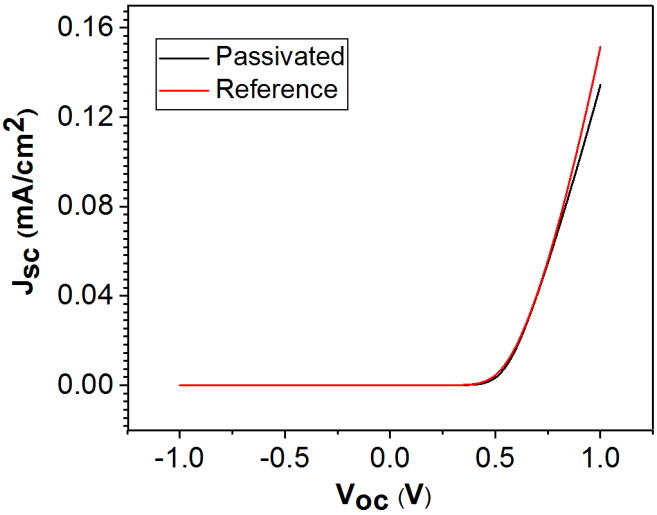

Figure 4.6: Good diode behavior is observed for the devices, with no sign of shunting in the reference device.

4.3.1. Doping concentration

The doping concentration (majority charge carrier density) is a vital parameter in a solar cell as, an adequate majority carrier concentration (10^{16}cm^{-3}-10^{17}cm^{-3}) would lead to satisfactory fermi-level splitting, thus not limiting the cell performance in anyway. To find the apparent doping concentration, conductance-voltage (CV) measurements were taken for both the devices. As mentioned earlier, the SLG substrate has an alkali barrier layer which prevents the diffusion of Na from the SLG into the absorber. Thus, to avoid the so called 'roll over' effect [61] for the passivated device, an ultra-thin NaF (3-4 nm) layer is deposited before the CIGS deposition (for both the devices). Logically, the amount of Na should be similar in both the passivated and reference device. C-V measurements were then performed on both completed devices for a bias voltage ranging from -2 V to 0.5 V with the frequency varying from 10^3 Hz to 10^6 Hz. The doping concentration is then extracted at 0 V for a set frequency for both the devices. The values were found to be similar for both the devices; 1.9×10^{16} cm^{-3} for the reference device and 1.1×10^{16} cm^{-3} for the passivated device (seen in Figure 4.7). This would suggest that the Na concentration are identical in both the devices. This is important as alkali metals like sodium improve the electrical performance of a CIGS device; incorporating Na into the absorber via a NaF precursor layer (ultra-thin layer 15-20 nm) improves the V_{OC} by 1 mV and the carrier concentration by a factor of 10^{16}cm^{-3} [52].

In the present case, the difference in the carrier concentration is nearly 0.8×10^{-16}cm^3, which could marginally improve the V_{OC} for the reference device (using Equation 4.4, the difference in the V_{OC} was calculated to be 14 mV) when compared to the passivated device.

$$\Delta V_{OC} = \frac{K_B T}{q} \ln\left(\frac{N_{ref}}{N_{pass}}\right) \tag{4.4}$$

Where,
N_{ref} = majority charge carrier concentration for the reference cell,
N_{pass} = majority charge carrier concentration for the passivated cell.

Considering the lower carrier concentration in the passivated device, it can be expected that the V_{OC} is reduced when compared to the reference device. Having a higher charge carrier concentration leads to an increased fermi level splitting, thus, the reference device should then have a higher open circuit voltage which is however not the case. From the above arguments, it can be concluded that the improvements in the cell V_{OC} cannot be linked to the difference in the carrier concentration or the amount of Na in the CIGS absorber.

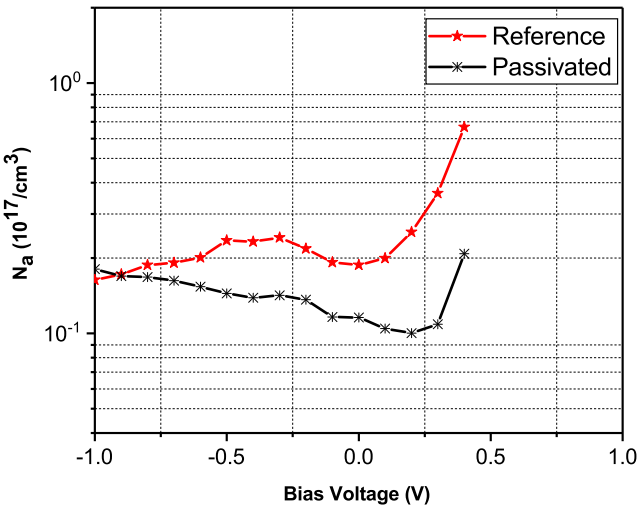

Figure 4.7: A higher majority charge carrier was obtained for the reference device. This could be due the variation in sodium or copper content in both the cells and can also contribute to a higher V_{OC} in the reference device.

4.3.2. Increased Shunt Resistance

The shunt resistances were extracted from the JV measurements of the respective devices and found to be 400 Ωcm^2 for the reference device while for the passivated cell, it was found to be close to 716 Ωcm^2 (Figure 4.8). In general, lower shunt resistances have been reported for thin-CIGS devices as the as-deposited surface roughness of the CIGS absorber is similar to the film thickness [55]. The higher shunt resistance for the passivated device suggests that the Al_2O_3 layer reduces shunt paths through the CIGS layer and/or lessens the pinholes.

Yet, the increase in the shunt resistance is too low to explain the obtained improvements in the open circuit voltage. It does to a certain extent, explain the slightly higher fill factor obtained for the passivated device.

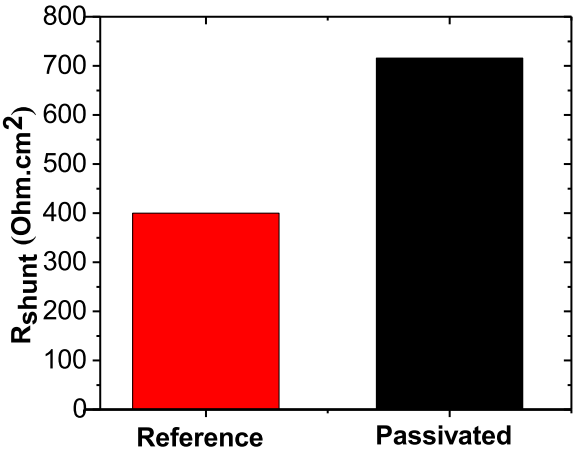

Figure 4.8: An improved shunt resistance is observed for the passivated device suggesting that the Al_2O_3 layer suppresses shunt paths and pin holes in the absorber.

4.3.3. Reduced dark saturation current density

The dark saturation current density was extracted from the JV measurements (analysed using the one-diode model) from the respective devices. It was found to be nearly 2 orders lower for the passivated device when compared to the reference cell; (1.45×10^{-8}Acm^{-2}) for the reference and (2.2×10^{-6}Acm^{-2}) for the passivated (Figure 4.9b).

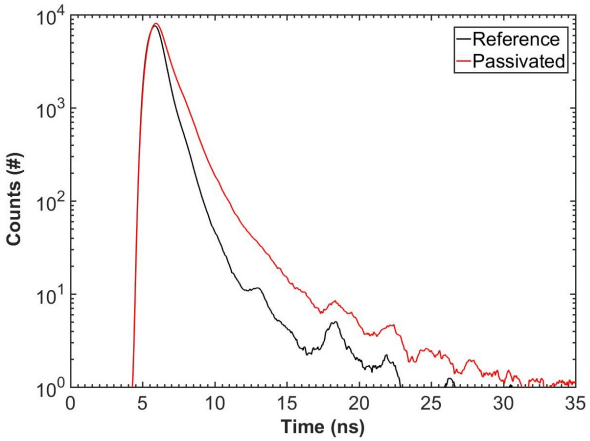

(a) Time resolved photoluminescence

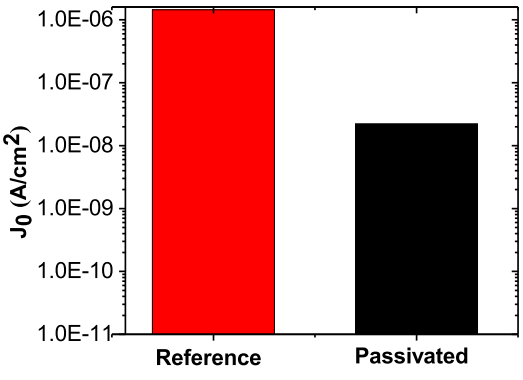

(b) Dark saturation current density

Figure 4.9: The obtained longer charge carrier life-time and decreased dark saturation current density (nearly 2 times) correlates to the obtained improvements in the V_{OC} for the passivated cell.

This indicates that the carrier recombination has reduced in the passivated device, which could have been due to the bulk and/or the interface surfaces. Since the bulk of the absorber and front interface stay unchanged for both the devices, it is more likely that it is the rear interface (reduced rear-surface recombination) that has impacted the dark saturation current. This was further supported by temperature dependent V_{OC} measurements (not shown here); the extrapolated V_{OC} at 0K was 1.15 eV for the passivated device, thus the activation energy of the dominant recombination path was equal to the bandgap of the material (from PL measurement) suggesting that the bulk recombination is more limiting than the interface. Moreover, the front interface (CIGS/CdS) is predicted to have a slightly positive conduction band offset (a "spike"), therefore, it is more likely that the limitation is due to the CIGS/Mo interface. The TRPL measurements (seen in Figure 4.9a) also shows a slight improvement in the charge carrier recombination, however, since a 1-stage co-evaporation process was used in the present case, a significant improvement is not seen.

4.3.4. Photoluminescence spectrum analysis

In this segment, the studies performed to understand the impact of the passivation layer on the photoluminescence spectra are explained. The PL experiments were performed on a completed solar cell consisting of Mo/CIGS/CdS stack(reference) and Mo/Al_2O_3 (6±1 nm)/CIGS/CdS (passivated) with a 532 nm laser. For thin-CIGS absorbers, the charge carriers are created throughout the absorber. Hence, the PL signal sensitive to the entire CIGS volume, which was also seen in the current research work (Figure 4.10) as there is a change in the PL spectrum for a modified back surface solar cell. The intensity of a photoluminescence (PL) spectra decreases as non-radiative recombination increases. Non-radiative recombination, for most thin-film materials, occurs via defect states in the band gap. Thus, for a passivated solar device, it can be expected that the peak intensity of the PL curve be enhanced. As expected, the PL signal is significantly higher for the passivated device when compared to the reference; the peak intensity is 8 times higher in the passivated device.

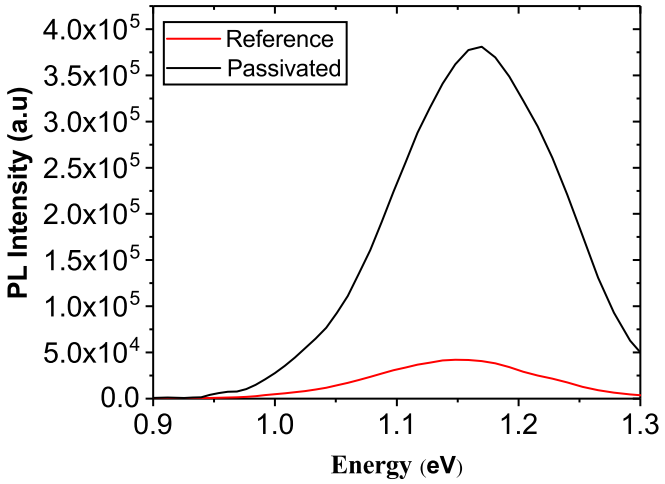

Figure 4.10: The intensity of the PL peak is nearly 8 times higher for the passivated device when compared to the reference device. An amplified PL spectra would suggest that non-radiative recombination is significantly reduced and that the fermi-level spitting is more enhanced. Thus, higher open-circuit voltages were obtained for the rear-passivated device.

To quantify the effects of the passivation layer on the open-circuit voltage, the methods highlighted by Mollica et al. [37] was used.

The yield of a photoluminescence spectrum can be obtained from Generalized Planck's Law, given by Equation 4.5.

$$Y_{PL} \propto \int_{E_G}^{\infty} \mathrm{E}^2 \frac{\mathrm{d}E}{\exp\left(\frac{E-\mu}{kT}\right) - 1} \tag{4.5}$$

Where,
Y_{PL}= PL Yield,
E_G= Band-gap of the material,
E= energy of emitted light,
μ= chemical potential of an electron - hole pair.

For a sufficiently illuminated solar device, the term $\left(\frac{E-\mu}{kT}\right) \gg 1$. Now analytically solving Equation 4.5 with the above approximation, the following equation is obtained.

$$Y_{PL} = B.\exp\left(\frac{\mu}{kT}\right) \tag{4.6}$$

Here B is a proportionality constant dependent on the temperature and band gap of the material. Now, from Equation 4.6, the change in the chemical potential can be obtained leading to Equation 4.7.

$$\Delta\mu = kT.\ln\frac{Y_{PL}^{Al_2O_3}}{Y_{PL}^{Mo}} \tag{4.7}$$

Where,
$Y_{PL}^{Al_2O_3}$= PL yield of the sample with a rear Al_2O_3 passivation layer,
Y_{PL}^{Mo}= PL yield for the plain-reference sample.

From Equation 4.7, the change in the PL-yield can be correlated to the change in the chemical potential. Since the chemical potential is equivalent to separation of the quasi fermi energy level, the value of $q.\Delta\mu$ should be the observed increase in cell V_{OC} or its upper limit in mV. Substituting the values in Equation 4.7 (the peak intensity was 8 times the reference), the change in the chemical potential times elementary charge was found to be around 54 mV. Interestingly, such an improvement in the V_{OC} was seen for the passivated device. The improvement in the PL spectrum is too large to be related to only the optical effects of the passivation layer, thus the Al_2O_3 improves the opto-electrical characteristics of the cell (improved interface quality). This can be explained as follows; the fermi-level splitting depends on the product of both the majority and minority charge carrier concentrations. Since the majority carrier concentration is identical in both the devices, this means that the minority carrier collection probability improved. This could be due to 1) increase in the diffusion length of the minority carrier due to added drift-field (electrons generated beyond the space charge region will drift towards the it [30]) and 2) reduced minority charge carrier recombination at the rear interface (lower surface recombination velocity). Thus, from the PL analysis, it is concluded that the nano-patterned Al_2O_3 layer decreases the number of active non-radiative defects in the CIGS device and thus reduces the rear interface recombination.

4.3.5. Conclusions

In summary, an advanced architecture to integrate a rear surface passivation scheme in a thin-CIGS solar device was demonstrated. The modified rear surface consisted of an ultra-thin passivation layer with nano-size localized openings on its surface. A simple and technologically feasible method was demonstrated to generate these nano-sized point openings without the fill factor being affected severely. Statistical data of over 25 cells suggest that the passivation layer reduces the rear interface recombination significantly when compared to the reference device. For the same band gap, the open-circuit voltage deficit reduced from 615 mV to 553 mV by implementing these passivation schemes. Higher efficiencies were thus obtained owing to higher fill factors and open-circuit voltages, bringing down the efficiency drop when compared to a standard CIGS device. Analyses of the PL spectra, TRPL and temperature dependent V_{OC} measurements further support the positive impacts of passivation layer; i) it reduces the rear interface defects ii) it lowers the rear interface recombination and iii) it improves the minority carrier diffusion lengths.

5

Ag in passivated CIGS solar cells

In this chapter, the results of experiments performed for the development of Ag incorporated CIGS solar cells are presented. These cells are still in their very early stages of development and further studies would be performed to characterize, optimize and develop these cells. Hence, only a limited number of experiments were performed and are presented here. This work received funding from the European Union's H2020 research and innovation program under grant agreement No. 715027.

5.1. Initial Trials

To obtain further efficiency improvements in a polycrystalline CIGS absorber, two approaches are now being researched (other than device optimization): 1) band-gap widening (from 1.1 to 1.4 eV) 2) tandem solar cells architectures (to optimize absorption of incoming solar spectra). For conventional CIGS solar cells, wider band gaps can be obtained by increasing the gallium content (GGI) in the cell [28]. Typically, wider bandgaps lead to higher open circuit voltages, which can reduce the I^2R losses (reduced current) and thus, the thickness of the TCO layer [66]. Yet, if the GGI ratio is greater than 0.3, the performance of the device degrades, limiting the maximum achievable bandgap for the device [63]. An example of the same can be the open-circuit deficiency problem; the V_{OC} of the cell does not scale as the band gap increases. Needless to say, this effects the cell efficiency, which can hinder the development of chalcopyrite PV . Recently, the alloying of silver into a CIGS absorber has gained interest as an alternative; it reduces the defect density, lowers the structural disorder and increases the open circuit voltage for wider band-gap energies of upto 1.4 eV [27, 67]. For example, Nakada et al. [40] showed that for Ag $(In_{1-y}Ga_y)Se_2$ (AIGS) solar cells, open circuit voltages as high as 949 mV were obtainable for sound cell efficiencies of 9.3%. Having the same structure (Ag substituting Cu), the alloying of silver in the CIGS solar cell yields wider-band gaps with good electrical performance. Hence, AIGS photovoltaic devices appear to be interesting. Thus, an attempt was made to incorporate silver into the CIGS solar cell. The beneficial effects of alloying silver into the absorber has been investigated extensively by IEC thus, the details of crystal structure, electrical and optical properties etc. can be found elsewhere [16–18, 54, 60]. Also, in the present work, only a generalized and preliminary study of silver incorporation in a rear passivated CIGS absorber has been provided. Since this a new concept, only the latest work performed by the thin-film team at IMEC, is presented and explained here. Extensive studies are being carried out to further optimize and develop wider band-gap AIGS solar cell by the same group. Silver is usually incorporated into the CIGS absorber during the co-evaporation process: by adding an extra Ag source in the co-evaporation chamber. Here, an alternative approach is suggested. Yin et al. [68] reported that silver nano-particles at the rear surface of the cell tend to diffuse into the bulk CIGS during the high temperature absorber deposition step.

Furthermore, a 50 nm Al_2O_3 was needed to thermally passivate the diffusion of silver into the absorber, with anything less being ineffective. In our case, this can be used to our advantage; a thin passivation layer (6 $\pm$1 nm Al_2O_3) can be used to reduce the interface recombination while silver can diffuse into the absorber from the rear surface. More importantly, the silver particles were needed for contact creation as explained in the next section. Accordingly, studies began to fabricate Ag nano-particles on a Mo/SLG substrate.

5.2. Annealing Experiments

A 10-15 nm ultra-thin film of silver was evaporated on to the surface of the SLG substrate. To generate the nano-particles, the silver coated substrates were annealed in a nitrogen environment. Though, for silver diffusion, the size of the nano-particles may not be of that importance, it can play a role if other factors like contact creation and light trapping were considered. The concept of light trapping is interesting as 1) metallic nano-structures like Ag have pronounced localized surface plasmons 2) light scattering due to the nano-particles can enhance the short circuit current which is one of the limiting parameters for a thin-CIGS device. Thus, taking the above factors into consideration, nano-particles of about 500 nm in diameter were targeted (as explained in the earlier chapters, for electrical contacts, particles of a few hundred nm are ideal). The annealing temperature and annealing time play an important role in controlling the size and surface coverage of the nano-particle. Initially, experiments were performed to investigate the effect of annealing parameters (temperature, time, ramp up speed, cool down time etc.) on the size and surface coverage of the nano-particles. Post experimentation, it was found that, a temperature of 350-375°C and an annealing time of about 30 minutes yielded particles in the range of 500-600 nm with a surface coverage ranging from 5-10% (Figure 5.1). As the annealing temperature is way below the melting point of silver, it can be assumed that there is no material wastage. Thus, a reduction in the surface coverage can correspond to the increased height of the generated nano-particles.

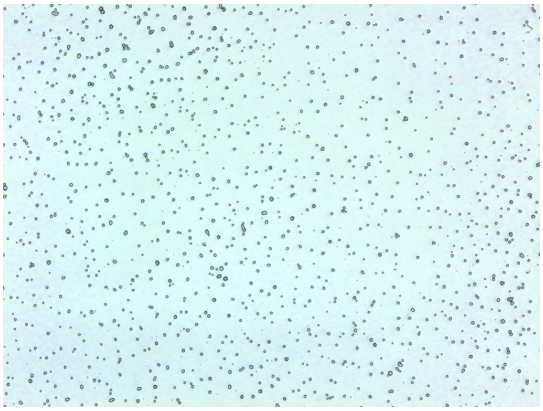

(a) Ag particles after 25 minutes at 350°C.

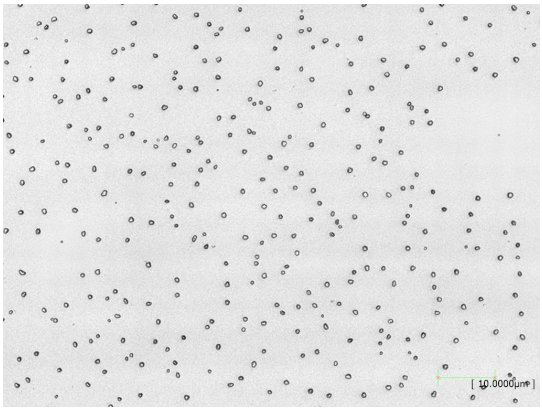

(b) Ag particles after 30 minutes at 375°C.

Figure 5.1: Microscopic images of a SLG substrate demonstrating the effects of annealing parameters like temperature and time on the size of the Ag nano-particles.

5.3. Cell Integration

In the earlier case the CdS NPs used to create the contacts, were removed from the surface. In this case however, it is necessary that the Ag NPs stay on the surface. Thus, initially, the ALD deposition parameters were varied drastically to try and obtain non-conformal ALD growth. In doing so, it is possible that some regions of the cell or regions around complex 3-D structures (like the nano-particles) may or/and may not be uniformly coated, which could generate contacts.

The idea for non-conformal ALD growth can be explained as follows; in an idealized temperature window for ALD deposition, the growth per cycle (GPC) is weakly dependent on the temperature [47]. However, outside that temperature window, the idealized ALD behaviour can be lost due to the following reasons i) condensation: precursor gases can condense on the substrate surface which could prevent efficient purging ii) lower temperature: limits completion of precursor reactions due to insufficient reactivity and iii) desorption: the deposited film or the precursor gases may desorb from the surface, effecting the GPC [47]. Thus, a trial device was fabricated with an ultra-thin non-conformally grown Al_2O_3 layer (5 nm) on the silver nano-particles (non-conformal parameters include-low temperature (from 150° to 100°C), reducing pulse time for the TMA precursor (from 0.016 to 0.006 seconds) etc). By analysing the results however, it was found that extremely low short current (roughly 11 mA/cm^2), high series resistance and extremely low shunt resistance were obtained (about 5 Ωcm^{-2} and 33 Ωcm^{-2} respectively). The high series resistance and poor carrier collection suggests that the contacts were not well defined or created properly. However, the fact that some current was extracted shows that some contacts were created. Yet, it is difficult to conclude if the contacts were a result of the non-conformal ALD or the pre-deposited NaF layer (now under research). Thus, non-conformal ALD cannot be used as a controllable and repeatable method to create contacts. However, it does show that even non-conformal ALD creates a stable layer which can withstand the harsh CIGS deposition conditions. A different approach was tested to create contacts and allow the Ag nano-particles to remain on the surface; to use of CdS nano-particles to create the contacts (as done in chapter 4). A modified cell architecture was applied to integrate Ag in a rear-passivated solar cell as explained in the table below.

Table 5.1: Fabrication steps for a modified thin-CIGS device with silver incorporation.

Step	Description
0	SLG/Mo cleaning
1	Thin Ag layer; evaporation
2	Ag-nano-particle ; Annealing
3	Particle rich CdS deposition; CBD
4	Al_2O_3 deposition; ALD
5	CdS particle removal; rear contact
6	NaF layer deposition
7	thin-CIGS deposition; 1-stg co-evaporation
8	Buffer layer (CdS); CBD
9	Window layer; RF sputtering
10	Ni/Al/Ni front contact; Evaporation

5.3.1. Results and discussion

A (A)CIGS device was fabricated based on the modified fabrication steps mentioned in Table 5.1. The deposition was done with slightly copper poor conditions to reduce the possibility of shunting in the device (for Cu+Ag/Ga+In >1, the device is heavily shunted). To be clear, in this run, 3 devices were fabricated, one being a plain reference device, the second being the passivated device (the results of the first and second have been explained in the previous chapter) and the Ag (passivated) device. The electrical characteristics of the reference device and Ag (passivated) device are presented in Figures 5.2 and 5.3. From the box plots, it is possible to see that there is an improvement in the open-circuit voltage (+28 mV) when compared to the reference, yet the increase is not as high as in the case of a plain passivated device obtained in the previous case. The reduced V_{OC} can be ascribed to the reduced doping concentration in the Ag (passivated) device (obtained from C-V measurements, in the range of 10^{15}cm^{-3}), even lower than what was obtained for the passivated

device. Low doping can be possibly attributed to two factors: 1) Ag occupies interstitial positions where they act as compensating donors, 2) due to electrically active states at the front interface [8](however Drive-Level Capacitance Profiling measurements were not performed to confirm the same). The fill factor was also reduced when compared to the passivated device; an average of 60% was obtained. This could be due to the CdS NP removal step; during the CdS nano-particle removal, even silver nano-particles could have partially been removed from the surface. Thus, the electrical contact area is increased and/or sub-optimized, which effects the fill factor.

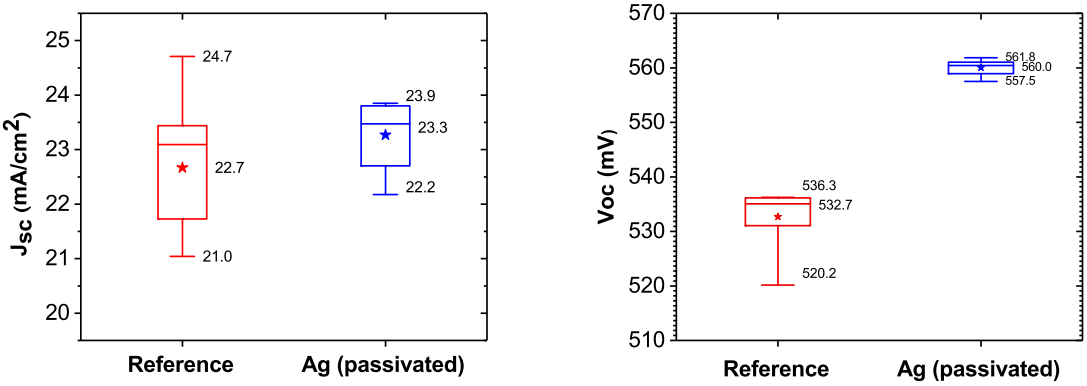

(a) The short circuit increased, possibly due to reduced structural disorder in the crystal lattice.

(b) Open circuit voltage for both the devices.

Figure 5.2: Effect of silver inclusion on the V_{OC} and J_{SC}.

This is also reflected in the higher average series resistance for the cell; 2.4 Ωcm^{-2}. The reduced V_{OC} and FF led a slightly reduced efficiency of 7.8% when compared to the passivated device, yet it was still higher than the reference device, Figure 5.3b. An important trend observed is the improvement in the short circuit current (+0.6 mA/cm^2).The higher J_{SC} is also seen in the EQE curves, where there is an improvement in the entire solar spectrum (Figure 5.4).

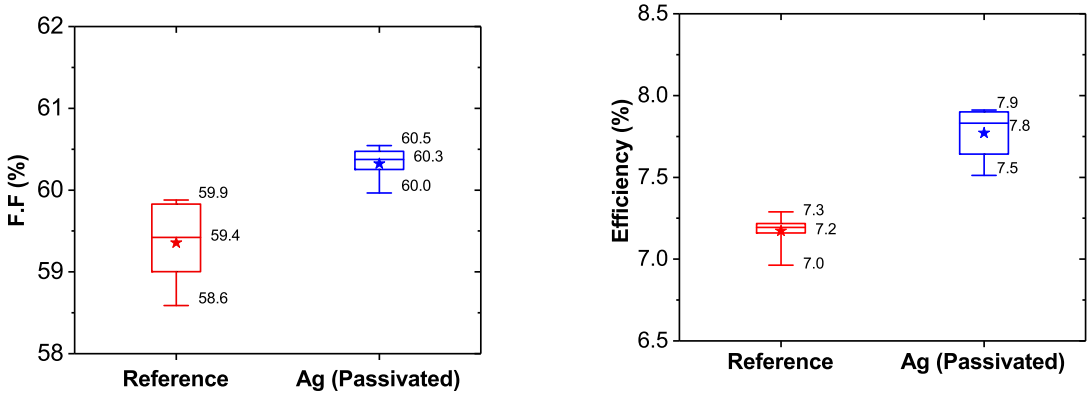

(a) Fill Factor comparison.

(b) Efficiency comparison.

Figure 5.3: Effect of Ag inclusion in a rear passivated device.

Though it is difficult to give conclusive reasons for the same, it is possible that the combined effects of the passivation layer and bulk improvement due to Ag diffusion (hence an improved EQE spectra in the visible light region) improved the average J_{SC}. However, further studies are needed to explain the same. This is because, Ag has a low diffusion coefficient, hence higher temperatures are needed to promote the diffusion of silver into the absorber. Since, in the present case, the CIGS deposition conditions were not varied significantly (for example the deposition temperature remained unchanged), it is more likely that the silver did not or partially diffused into the absorber (due to low thickness of the CIGS absorber).

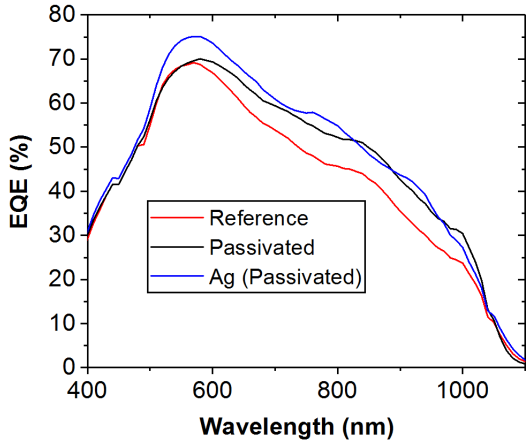

Figure 5.4: The EQE curves for the three device tested in the current research work. For the Ag(passivated) device, an improvement in the bulk and infra-red region can be seen.

The PL spectrum of the Ag (passivated) device was amplified when compared to the reference (Figure 5.5), however, it is more likely that it is a result of the passivation layer. The reduced PL intensity would suggest an increased non-radiative recombination most likely due to the irregular silver diffusion. Moreover, a part of the Ag could have been etched off the surface along with the CdS particles during the contact creation step. This partially explains the reason for acceptable shunt resistances obtained from cell measurements contrary to usually low shunt resistances reported by various authors.

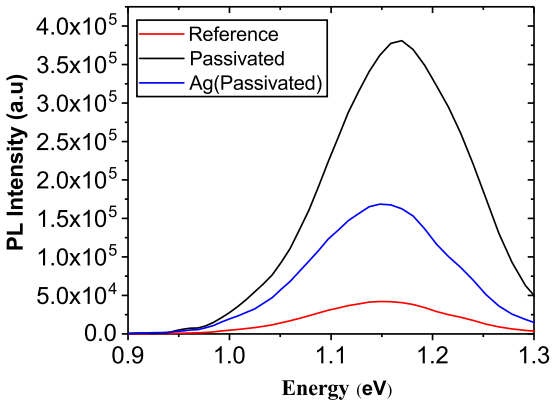

Figure 5.5: A reduced PL intensity for the Ag (passivated) device would suggest that additional recombination centres or defect states were created.

5.4. Conclusion

For obtaining high quality Ag (passivated) devices, the uniformity of Ag in the absorber is essential, which in this case couldn't have been achieved. The band-gap of the Ag (passivated) device did not increase, as seen from the PL curve and the EQE, further proof of the lack of sufficient silver in the absorber. Furthermore, from the C-V measurements, it is observed that the doping concentration was reduced significantly (by 1 order), thus, alkali treatments would be needed to improve the doping concentrations. Accordingly, moderate efficiencies were thus obtained (on average 7.8%) owing to the marginal improvements in the FF, J_{SC} and V_{OC}. Furthermore, advanced optical techniques like E-BIC would be needed to find the uniformity of the Ag diffusion into the absorber. Additionally, silver alloying is known to improve the grain size which can improve cell performance. In the present case, such comparisons and studies were not performed as the uniform diffusion of silver into the absorber is itself doubtful. Hence, more optimization and characterization studies would be needed.

6

Concluding Remarks and Outlook

6.1. Conclusions

CIGS is a complex tertiary compound but an excellent semiconductor device for solar cell applications. Given the potential for high efficiency devices and gigawatt scale growth, thin-CIGS solar cells would aid in increasing the throughput and reducing the overall cell cost. Yet, poor light absorption and increased interface recombination lowers the power conversion efficiency. To reduce the rear-surface recombination, in the present work, the cell architecture is modified by the implementation of an ultra-thin passivation layer. The choice of the passivation layer was based on parameters like interface passivation qualities (for example adhesion, thermal stability etc.), industrial viability (large scale deployment), ease of deposition (for example temperature, thickness control etc.) and its adaptability to the p-type nature of the CIGS layer. An Al_2O_3 layer was used for the same reasons, however being a non-conductive layer, point contacts were created using nano-particles. Significant improvements in the open circuit and efficiency were obtained because of a rear passivation layer with well-spaced and randomized nano point contacts. A maximum V_{OC} of 604 mV was obtained by the implementation of this modified cell architecture with the non-radiative recombination reducing by a factor 8 as seen from the PL spectra. A detailed analysis of the diode characteristics, photoluminescence peaks and EQE curves suggests that the passivation layer improves the opto-electrical properties of the cell. Furthermore, the results were reproducible, showing that the nano-particle approach to create point-nano contacts was technically possible. However low J_{SC} and moderate fill factors still limit the device performance, thus optical confinement techniques need to be considered. Furthermore, a new and untested method of silver addition is suggested, with the initial studies having promising results.

6.2. Outlook

In the present case closely (1-3 μm) spaced nano-contacts worked fine however, multiple factors such as the quality of the absorber (diffusion length), sodium content, absorber thickness and lateral carrier resistance can affect the electrical contacting. Hence, further work should be done towards understanding and optimizing the point contact design. Similarly, CdS nano-particles were used to creating point-openings in this case however, other types of nano-particles like plastic or glass nano-beads should also be tested. This would reduce the use of toxic CdS, which can be a potential issue. The nano-particle approach to create contacts has the potential for industrial viability, hence efforts towards this direction would help the CIGS community. Additionally, there were limitations in the thickness of the Al_2O_3 due blistering issues and inefficient contact creation. However, other deposition methods like PECVD or DC sputtering can be perfected for good interface quality without the issue of blistering for thicker layer.

Furthermore, use of nano-rods can be tested for contact creation due to potential advantages like 1) use of thicker passivation layers and 2) lift-off method to remove the nano-rods. Hence, there lies a potential scope for improvement in this aspect. Additionally, grain refinement is an important aspect of the cell that needs to be improved. For this 3-stage CIGS deposition techniques can be implemented or silver alloying can be used among others. Yet, it is important to control the CGI ratio during silver addition as excess silver can shunt the device. Alloying of silver must be done during the CIGS deposition process rather than using the approach used in this method. A much better control on the final silver content in the cell can obtained by this method. Moreover, tandem cells can be made using AIGS top cell (greater band-gap) and CIGS bottom cell (lesser band-gap).

Bibliography

[1] KW Böer. Payback of solar systems. *Solar energy*, 20(3):225–232, 1978.

[2] Adrian Chirilă, Patrick Reinhard, Fabian Pianezzi, Patrick Bloesch, Alexander R. Uhl, Carolin Fella, Lukas Kranz, Debora Keller, Christina Gretener, Harald Hagendorfer, Dominik Jaeger, Rolf Erni, Shiro Nishiwaki, Stephan Buecheler, and Ayodhya N. Tiwari. Potassium-induced surface modification of Cu (In,Ga) Se_2 thin films for high-efficiency solar cells. *Nature Materials*, 12:1107, 2013. doi: 10.1038/nmat3789https://www.nature.com/articles/nmat3789#supplementary-information. URL `http://dx.doi.org/10.1038/nmat3789`.

[3] European Commission. Communication from the commission to the European parliament, the council, the European economic and social committee and the committee of the regions, on the review of the list of critical raw materials for the EU and the implementation of the raw materials initiative. `https://ec.europa.eu/growth/sectors/raw-materials/specific-interest/critical_en`, Online, accessed on: 25 May 2018.

[4] Miguel A Contreras, B Egaas, P Dippo, J Webb, J Granata, K Ramanathan, S Asher, A Swartzlander, and R Noufi. On the role of Na and modifications to Cu (In,Ga) Se_2 absorber materials using thin-MF (M= Na, K, Cs) precursor layers [solar cells]. In *Photovoltaic Specialists Conference, 1997., Conference Record of the Twenty-Sixth IEEE*, pages 359–362. IEEE, 1997.

[5] N. Dahan, Z. Jehl, T. Hildebrandt, J. J. Greffet, J. F. Guillemoles, D. Lincot, and N. Naghavi. Optical approaches to improve the photocurrent generation in Cu(In,Ga)Se_2 solar cells with absorber thicknesses down to 0.5 μm. *Journal of Applied Physics*, 112(9), 2012. ISSN 0021-8979. doi: Artn09490210.1063/1.4762004. URL `<GotoISI>://WOS:000311968400134https://aip.scitation.org/doi/pdf/10.1063/1.4762004`.

[6] MJ Mariska de Wild-Scholten. Energy payback time and carbon footprint of commercial photovoltaic systems. *Solar Energy Materials and Solar Cells*, 119:296–305, 2013.

[7] Alan E Delahoy, Liangfan Chen, Masud Akhtar, Baosheng Sang, and Sheyu Guo. New technologies for CIGS photovoltaics. *Solar energy*, 77(6):785–793, 2004.

[8] Peter T Erslev, JinWoo Lee, Gregory M Hanket, William N Shafarman, and J David Cohen. The electronic structure of $CuInSe_2$ alloyed with silver. *Thin Solid Films*, 519(21):7296–7299, 2011.

[9] Rebekah L Garris, Steve Johnston, Jian V Li, Harvey L Guthrey, Kannan Ramanathan, and Lorelle M Mansfield. Electrical characterization and comparison of CIGS solar cells made with different structures and fabrication techniques. *Solar Energy Materials and Solar Cells*, 174: 77–83, 2018. ISSN 0927-0248.

[10] British Petroleum Global. BP statistical review of world energy. *London, 71st Edition, BP Statistical*, 2017.

[11] Markus Gloeckler and James R Sites. Potential of submicrometer thickness Cu(In,Ga)Se_2 solar cells. *Journal of Applied Physics*, 98(10):103703, 2005. ISSN 0021-8979.

[12] Simon Glöser, Luis Tercero Espinoza, Carsten Gandenberger, and Martin Faulstich. Raw material criticality in the context of classical risk assessment. *Resources Policy*, 44:35–46, 2015. ISSN 0301-4207.

[13] Martin A Green. *Solar cells: operating principles, technology, and system applications*. Prentice-Hall, Inc., Englewood Cliffs, NJ, 1982.

[14] Martin A Green. *Third generation photovoltaics: advanced solar energy conversion*, volume 12. Springer Science & Business Media, 2006.

[15] Richard Grey. The biggest energy challenges facing humanity. `http://www.bbc.com/future/story/20170313-the-biggest-energy-challenges-facing-humanity`, Online, accessed on: 25 May 2018.

[16] Gregory M Hanket, Jonathan H Boyle, and William N Shafarman. Characterization and device performance of (AgCu)(InGa)Se_2 absorber layers. In *Photovoltaic Specialists Conference (PVSC), 2009 34th IEEE*, pages 001240–001245. IEEE, 2009.

[17] Gregory M Hanket, Jonathan H Boyle, William N Shafarman, and Glenn Teeter. Wide-bandgap (AgCu)(InGa)Se_2 absorber layers deposited by three-stage co-evaporation. In *Photovoltaic Specialists Conference (PVSC), 2010 35th IEEE*, pages 003425–003429. IEEE, 2010.

[18] Gregory M Hanket, Christopher P Thompson, Jes K Larsen, Erten Eser, and William N Shafarman. Control of ga profiles in (AgCu)(InGa)Se_2 absorber layers deposited on polyimide substrates. In *Photovoltaic Specialists Conference (PVSC), 2012 38th IEEE*, pages 000662–000667. IEEE, 2012.

[19] Steven S Hegedus and William N Shafarman. Thin-film solar cells: device measurements and analysis. *Progress in Photovoltaics: Research and Applications*, 12(2-3):155–176, 2004.

[20] Kelsey AW Horowitz and Michael Woodhouse. Cost and potential of monolithic CIGS photovoltaic modules. In *Photovoltaic Specialist Conference (PVSC), 2015 IEEE 42nd*, pages 1–6. IEEE, 2015. ISBN 1479979449.

[21] Tung-Po Hsieh, Chia-Chih Chuang, Chung-Shin Wu, Jen-Chuan Chang, Jhe-Wei Guo, and Wei-Chien Chen. Effects of residual copper selenide on $CuInGaSe_2$ solar cells. *Solid-State Electronics*, 56(1):175–178, 2011.

[22] W. W. Hsu, J. Y. Chen, T. H. Cheng, S. C. Lu, W. S. Ho, Y. Y. Chen, Y. J. Chien, and C. W. Liu. Surface passivation of Cu(In,Ga)Se_2 using atomic layer deposited Al_2O_3. *Applied Physics Letters*, 100 (2), 2012. ISSN 0003-6951. doi: Artn02350810.1063/1.3675849. URL `<GotoISI>://WOS:000299126800088https://aip.scitation.org/doi/pdf/10.1063/1.3675849`.

[23] Fraunhofer ISE. Photovoltaics report. *Fraunhofer Institute for Solar Energy Systems ISE, Freiburg/Germany*, 2017.

[24] Philip Jackson, Roland Wuerz, Dimitrios Hariskos, Erwin Lotter, Wolfram Witte, and Michael Powalla. Effects of heavy alkali elements in Cu(In,Ga)Se_2 solar cells with efficiencies up to 22.6%. *physica status solidi (RRL)-Rapid Research Letters*, 10(8):583–586, 2016.

[25] Enrico Jarzembowski, Thomas Schneider, Bodo Fuhrmann, Hartmut Leipner, Wolfgang Fränzel, and Roland Scheer. Enhanced light management in Cu(In,Ga)Se_2 solar cells by structured rear contacts. In *Optical Nanostructures and Advanced Materials for Photovoltaics*, page PW3B. 4. Optical Society of America, 2016.

[26] Z Jehl, F Erfurth, N Naghavi, L Lombez, I Gerard, M Bouttemy, P Tran-Van, A Etcheberry, G Voorwinden, B Dimmler, et al. Thinning of CIGS solar cells: Part ii: Cell characterizations. *Thin solid films*, 519(21):7212–7215, 2011.

[27] Kihwan Kim, Seung Kyu Ahn, Jang Hoon Choi, Jinsoo Yoo, Young-Joo Eo, Jun-Sik Cho, Ara Cho, Jihye Gwak, Soomin Song, Dae-Hyung Cho, et al. Highly efficient ag-alloyed $CuInSe_2$ solar cells with wide bandgaps and their application to chalcopyrite-based tandem solar cells. *Nano Energy*, 48:345–352, 2018.

[28] R. Kotipalli, B. Vermang, V. Fjällström, M. Edoff, R. Delamare, and D. Flandre. Influence of Ga/(Ga + In) grading on deep-defect states of $Cu(In,Ga)Se_2$ solar cells. *Physica Status Solidi-Rapid Research Letters*, 9(3):157–160, 2015. ISSN 1862-6254. doi: 10.1002/pssr.201510024. URL <GotoISI>://WOS:000351674600001https://onlinelibrary.wiley.com/doi/abs/10.1002/pssr.201510024.

[29] R. Kotipalli, B. Vermang, J. Joel, R. Rajkumar, M. Edoff, and D. Flandre. Investigating the electronic properties of Al_2O_3/$Cu(In,Ga)Se_2$ interface. *AIP Advances*, 5(10), 2015. ISSN 2158-3226. doi: Artn10710110.1063/1.4932512. URL <GotoISI>://WOS:000364228800001https://aip.scitation.org/doi/pdf/10.1063/1.4932512.

[30] R Kotipalli, Olivier Poncelet, G Li, Y Zeng, LA Francis, Bart Vermang, and Denis Flandre. Addressing the impact of rear surface passivation mechanisms on ultra-thin $Cu(In,Ga)Se_2$ solar cell performances using SCAPS 1-D model. *Solar Energy*, 157:603–613, 2017.

[31] J. Krc, M. Sever, A. Campa, Z. Lokar, B. Lipovsek, and M. Topic. Optical confinement in chalcopyrite based solar cells. *Thin Solid Films*, 633:193–201, 2017. ISSN 0040-6090. doi: 10.1016/j.tsf.2016.08.056. URL <GotoISI>://WOS:000404802300037.

[32] Leeor Kronik, David Cahen, and Hans Werner Schock. Effects of sodium on polycrystalline $Cu(In,Ga)Se_2$ and its solar cell performance. *Advanced Materials*, 10(1):31–36, 1998.

[33] Zacharie Jehl Li-Kao, Negar Naghavi, Felix Erfurth, Jean François Guillemoles, Isabelle Gérard, Arnaud Etcheberry, Jean Luc Pelouard, Stephane Collin, Georg Voorwinden, and Daniel Lincot. Towards ultrathin copper indium gallium diselenide solar cells: proof of concept study by chemical etching and gold back contact engineering. *Progress in Photovoltaics*, 20(5):582–587, 2012. ISSN 1062-7995. doi: 10.1002/pip.2162. URL <GotoISI>://WOS:000306898200011https://onlinelibrary.wiley.com/doi/pdf/10.1002/pip.2162.

[34] Olle Lundberg. *Band gap profiling and high speed deposition $Cu(In,Ga)Se_2$ for thin film solar cells*. PhD thesis, Acta Universitatis Upsaliensis, 2003.

[35] J. Malmstrom, O. Lundberg, and L. Stolt. Potential for light trapping in $Cu(In,Ga)Se_2$ solar cells. *Proceedings of 3rd World Conference on Photovoltaic Energy Conversion, Vols a-C*, pages 344–347, 2003. URL <GotoISI>://WOS:000222658800092.

[36] Josephine Mason. China to plow $361 billion into renewable fuel by 2020. https://www.realclearenergy.org/2017/01/07/china_to_plow_361_billion_into_renewable_fuel_by_2020_280949.htmlP, Online, accessed on: 25 May 2018.

[37] Fabien Mollica. *Optimization of ultra-thin $Cu(In,Ga)Se_2$ based solar cells with alternative back-contacts*. PhD thesis, Université Pierre et Marie Curie-Paris VI, 2016.

[38] David Muñoz-Rojas, Viet Huong Nguyen, César Masse de la Huerta, Sara Aghazadehchors, Carmen Jiménez, and Daniel Bellet. Spatial atomic layer deposition (SALD), an emerging

tool for energy materials. Application to new-generation photovoltaic devices and transparent conductive materials. *Comptes Rendus Physique*, 18(7-8):391–400, 2017. ISSN 1631-0705. doi: 10.1016/j.crhy.2017.09.004. URL <GotoISI>://WOS:000416698000005https://www.sciencedirect.com/science/article/pii/S1631070517300567?via%3Dihub.

[39] Tokio Nakada. CIGS-based thin film solar cells and modules: Unique material properties. *Electronic Materials Letters*, 8(2):179–185, 2012.

[40] Tokio Nakada, Keiichiro Yamada, Ryota Arai, Hiroki Ishizaki, and Naoomi Yamada. Novel wide-band-gap Ag ($In_{1-x}Ga_x$) Se_2 thin film solar cells. *MRS Online Proceedings Library Archive*, 865, 2005.

[41] David W Niles, Kannan Ramanathan, Falah Hasoon, Rommel Noufi, Brian J Tielsch, and Julia E Fulghum. Na impurity chemistry in photovoltaic CIGS thin films: Investigation with x-ray photoelectron spectroscopy. *Journal of Vacuum Science & Technology A: Vacuum, Surfaces, and Films*, 15(6):3044–3049, 1997.

[42] W. Ohm, W. Riedel, U. Aksunger, D. Greiner, C. A. Kaufmann, M. C. Lux-Steiner, and S. Gledhill. Bifacial Cu(In,Ga)Se_2 solar cells with submicron absorber thickness: Back-contact passivation and light management. *2015 IEEE 42nd Photovoltaic Specialist Conference (PVSC)*, 2015. ISSN 0160-8371. URL <GotoISI>://WOS:000369992903153.

[43] K. Orgassa, H. W. Schock, and J. H. Werner. Alternative back contact materials for thin film Cu (In,Ga) Se_2 solar cells. *Thin Solid Films*, 431:387–391, 2003. ISSN 0040-6090. doi: 10.1016/S0040-6090(03)00257-8. URL <GotoISI>://WOS:000183680500080.

[44] Mario Pagliaro, Rosaria Ciriminna, and Giovanni Palmisano. BIPV: merging the photovoltaic with the construction industry. *Progress in photovoltaics: Research and applications*, 18(1):61–72, 2010.

[45] J Palm, F Karg, H Schneider, K Kushiya, L Stolt, AN Tiwari, E Niemi, M Beck, C Eberspacher, P Wohlfart, et al. White paper for CIGS thin film solar cell technology, 2017.

[46] Tiseva Plamena. Solar frontier reaches 22.9% efficiency on thin-film CIS cell. https://renewablesnow.com/news/solar-frontier-reaches-229-efficiency-on-thin-film-cis-cell-595223/, Online, accessed on: 25 May 2018.

[47] H. B. Profijt, S. E. Potts, M. C. M. van de Sanden, and W. M. M. Kessels. Plasma-assisted atomic layer deposition: Basics, opportunities, and challenges. *Journal of Vacuum Science & Technology A*, 29(5), 2011. ISSN 0734-2101. doi: Artn05080110.1116/1.3609974. URL <GotoISI>://WOS:000294482200002https://avs.scitation.org/doi/pdf/10.1116/1.3609974.

[48] IEA PVPS. Snapshot of global photovoltaic markets. *Report IEA PVPS T1-31*, 2017.

[49] E Płaczek-Popko. Top PV market solar cells 2016. *Opto-Electronics Review*, 2017. ISSN 1230-3402.

[50] Uwe Rau and Marion Schmidt. Electronic properties of ZnO/CdS/Cu(In,Ga)Se_2 solar cells—aspects of heterojunction formation. *Thin Solid Films*, 387(1-2):141–146, 2001.

[51] Uwe Rau and Hans-Werner Schock. Electronic properties of Cu (In,Ga) Se_2 heterojunction solar cells–recent achievements,current understanding, and future challenges. *Applied Physics A*, 69(2):131–147, 1999.

[52] P. M. P. Salomé, B. Vermang, R. Ribeiro-Andrade, J. P. Teixeira, J. M. V. Cunha, M. J. Mendes, S. Haque, J. Borme, H. Aguas, E. Fortunato, R. Martins, J. C. Gonzalez, J. P. Leitao, P. A. Fernandes, M. Edoff, and S. Sadewasser. Passivation of Interfaces in Thin Film Solar Cells: Understanding the Effects of a Nanostructured Rear Point Contact Layer. *Advanced Materials Interfaces*, 5(2), 2018. ISSN 2196-7350. doi: ARTN170110110.1002/admi.201701101. URL <GotoISI>://WOS:000423173800013https://onlinelibrary.wiley.com/doi/abs/10.1002/admi.201701101.

[53] M Schmid. Review on light management by nanostructures in chalcopyrite solar cells. *Semiconductor Science and Technology*, 32(4):043003, 2017. ISSN 0268-1242.

[54] William Shafarman, Christopher Thompson, Jonathan Boyle, Gregory Hanket, Peter Erslev, and J David Cohen. Device characterization of (AgCu)(InGa) Se $_2$ solar cells. In *Photovoltaic Specialists Conference (PVSC), 2010 35th IEEE*, pages 000325–000329. IEEE, 2010.

[55] WN Shafarman, RW Birkmire, S Marsillac, M Marudachalam, N Orbey, and TWF Russell. Effect of reduced deposition temperature, time, and thickness on Cu(In,Ga)Se_2 films and devices. In *Conference Record IEEE Photovoltaics Specialists Conference*, volume 26, pages 331–334. IEEE INC, 1997.

[56] Joseph Leo Shay and Jack Harry Wernick. *Ternary Chalcopyrite Semiconductors: Growth, Electronic Properties, and Applications: International Series of Monographs in The Science of The Solid State*, volume 7. Elsevier, 2017.

[57] William Shockley and Hans J Queisser. Detailed balance limit of efficiency of p-n junction solar cells. *Journal of applied physics*, 32(3):510–519, 1961.

[58] Arno HM Smets, O Isabella, M Zeman, et al. *Solar energy: the physics and engineering of photovoltaic conversion technologies and systems*. UIT, 2016.

[59] Piotr Szaniawski, Pedro Salomé, Viktor Fjällström, Tobias Törndahl, Uwe Zimmermann, and Marika Edoff. Influence of varying Cu content on growth and performance of Ga-graded Cu(In,Ga)Se_2 solar cells. *IEEE Journal of Photovoltaics*, 5(6):1775–1782, 2015.

[60] Yuki Tauchi, Kihwan Kim, Hyeonwook Park, and William Shafarman. Characterization of (AgCu)(InGa)Se_2 absorber layer fabricated by a selenization process from metal precursor. *IEEE Journal of Photovoltaics*, 3(1):467–471, 2013.

[61] B. Vermang, V. Fjällström, X. D. Gao, and M. Edoff. Improved rear surface passivation of Cu(In,Ga)Se_2 solar cells: A combination of an Al_2O_3 rear surface passivation layer and nano-sized local rear point contacts. *IEEE Journal of Photovoltaics*, 4(1):486–492, 2014. ISSN 2156-3381. doi: 10.1109/Jphotov.2013.2287769. URL <GotoISI>://WOS:000329038800073https://ieeexplore.ieee.org/ielx7/5503869/6684586/06662413.pdf?tp=&arnumber=6662413&isnumber=6684586.

[62] Bart Vermang, Hans Goverde, Loic Tous, Anne Lorenz, Patrick Choulat, Jorg Horzel, Joachim John, Jef Poortmans, and Robert Mertens. Approach for Al_2O_3 rear surface passivation of industrial p-type Si PERC above 19%. *Progress in Photovoltaics: Research and Applications*, 20(3):269–273, 2012.

[63] Su-Huai Wei, SB Zhang, and Alex Zunger. Effects of Ga addition to $CuInSe_2$ on its electronic, structural, and defect properties. *Applied physics letters*, 72(24):3199–3201, 1998.

[64] Wolfram Witte, Robert Kniese, and Michael Powalla. Raman investigations of Cu (In,Ga) Se_2 thin films with various copper contents. *Thin Solid Films*, 517(2):867–869, 2008.

[65] Colin A Wolden, Juanita Kurtin, Jason B Baxter, Ingrid Repins, Sean E Shaheen, John T Torvik, Angus A Rockett, Vasilis M Fthenakis, and Eray S Aydil. Photovoltaic manufacturing: Present status, future prospects, and research needs. *Journal of Vacuum Science and Technology A: Vacuum, Surfaces, and Films*, 29(3):030801, 2011.

[66] Zhang Xianfeng, Tsuyoshi Kobayashi, Yasuyoshi Kurokawa, Yoshiyuki Tashiro, Masahiro Ohtsuka, Tomoyuki Yamada, and Akira Yamada. Comparison of interface characterization between Ag (In, Ga) Se_2 and Cu (In, Ga) Se_2 solar cells by high-angle-annular dark-field scanning transmission electron microscopy. *Japanese Journal of Applied Physics*, 50(12R):126603, 2011.

[67] Keiichirou Yamada, Nobuyuki Hoshino, and Tokio Nakada. Crystallographic and electrical properties of wide gap Ag (In_{1-x}, Ga_x) Se_2 thin films and solar cells. *Science and Technology of Advanced Materials*, 7(1):42–45, 2006.

[68] Guanchao Yin, Alexander Steigert, Patrick Andrae, Manuela Goebelt, Michael Latzel, Phillip Manley, Iver Lauermann, Silke Christiansen, and Martina Schmid. Integration of plasmonic ag nanoparticles as a back reflector in ultra-thin Cu(In,Ga)Se_2 solar cells. *Applied Surface Science*, 355:800–804, 2015.

[69] SB Zhang, Su-Huai Wei, Alex Zunger, and H Katayama-Yoshida. Defect physics of the $CuInSe_2$ chalcopyrite semiconductor. *Physical Review B*, 57(16):9642, 1998.